# Modelling the Habitability of Exoplanets and Exomoons

Zachery McBrearty
Level 4 Project, MPhys Physics with Astronomy
Supervisor: Dr Richard Wilman
Second Supervisor: Dr Craig Testrow
Department of Physics, Durham University
Submitted: March 20, 2024

A 1-D energy balance climate model is developed in order to investigate how changing certain orbital or planetary parameters can result in changes to a planet's habitability. Theoretical relationships for temperature with respect to semi-major axis and eccentricity are derived from a 0-D energy balance model and are tested against the 1-D model and are found to be correct. A qualitative analysis of obliquity shows that there are optimal obliquities to minimise and maximise global temperature. The climates of Earth-like exomoons orbiting gas giants are also investigated, including reflected and emitted light from the gas giant, eclipsing, and tidal heating. The effect of these modifications are contrasted to the planetary model and the effects of varying the orbital parameters of the moon are also investigated and are found to be similar to corresponding planetary parameters but on smaller scales due to larger power laws.

## CONTENTS

## 1. INTRODUCTION

### A. Exoplanet and Exomoon Detection

When the first exoplanet was discovered is up for debate depending on classification [1]. To give a summary: The first evidence for an exoplanet came in 1988 but was attributed to stellar activity. This was followed up later in 2003 and found to be an exoplanet. This confirmation happened many years after 1992 when the first exoplanets were found orbiting a pulsar via the variations in pulsar timings due to those exoplanets. However, the intensity of radiation from these pulsars make life on these exoplanets impossible. Then the first potentially habitable exoplanets were found in 1995; potentially habitable because they orbit a Sun-like star.

Exoplanets are now found in a variety of indirect and direct methods. Indirect methods include pulsar timing, radial velocity, astrometry, and gravitational lensing. Direct methods include transits and direct imaging via coronagraph. Direct and indirect methods have also been combined to find planets. For example Kepler-88c was discovered indirectly due to variation in the transit of Kepler-88b [2].

These methods can also be extended to find exomoons around exoplanets. The pulsar timing from an exoplanet has additional variations due to an exomoon [3], and it has been shown that nearby exomoons may be found using Kepler (or Kelper-class) photometry by analysing variations in transit timing signals [4].

More recently, it has been shown that exomoons with strong tidal heating could be brighter than the exoplanet they orbit, so are easier to detect than exoplanets in some cases [5]. Further, the launch of the JWST has enabled the direct detection of earth-sized exomoons with economical use of observation time [6].

The culmination of all these methods is collated by the Encyclopaedia of Exoplanetary Systems [7] who report a total of 5641 exoplanets confirmed but no exomoons.

Reaching these exoplanets is a project for the far future, however current missions are building up to this auspicious goal. The one recent (and on going) mission is the Artemis Plan [8] which plans to build a Base Camp on the lunar surface and setup Gateway in lunar orbit. Additionally, the China National Space Administration also plan to return to the moon with the

International Lunar Research Station [9]. Both these projects will allow for human settlement away from the Earth, and are vital in progressing further out into our own solar system and beyond.

### B. Energy Balance Models

Analysing the habitability of exoplanets can be difficult. The Trappist-1 system is an excellent example. In the system seven Earth-like planets were found within the habitable zone of their host star [10]. However, they are not habitable due to a mixture of being tidally-locked to the star and experiencing extreme solar winds which have probably stripped them of any atmosphere long ago [11, 12]. This suggests that modelling of an exoplanet's habitability requires modelling of the dynamic atmosphere,

One way to model the exoplanets is with an energy balance model, where incoming energy (usually from a star) is equated to outgoing energy (usually blackbody emission). If no time dependence is considered then the 0-D Energy Balance Model (0DEBM) is

$$\pi r^2 S(1-A) = 4\pi r^2 \sigma T^4, \tag{1}$$

where $r$ is the radius of the planet, $S$ is the incoming solar radiation (insolation) which is reduced by the albedo of the planet $A$. The blackbody term is given by the Stefan-Boltzmann constant, $\sigma$, and the temperature of the planet $T$. This model does not resolve the planet's surface, and comes with a variety of assumptions such as energy being distributed equally over the entire planet's surface. This assumption implies that the planet is not tidally locked and has good diffusion mechanisms to spread out heat.

While this 0DEBM is powerful, there are limitations. The temperature produced is an average over time which means extreme temperatures are ignored. Additionally, different latitude bands experience different amounts of insolation depending on time and obliquity, thus the assumption of even energy distribution is not entirely valid. This is especially apparent on the Earth where the poles have much lower temperatures (i.e. freezing) compared to the equator.

These problems can be addressed with a 1-D Energy Balance Climate Model (1DEBCM). The 1DEBCM is given in latitude, $\lambda$, and time, $t$, coordinates as

$$C(\lambda,T)\frac{\partial T(t,\lambda)}{\partial t} = D\left[\frac{\partial^2 T(t,\lambda)}{\partial \lambda^2} - \tan\lambda \frac{\partial T(t,\lambda)}{\partial \lambda}\right] + S(\lambda,t)(1-A(T)) - I(T), \tag{2}$$

where $C$ is the heat capacity for a latitude band, $D$ is the diffusion constant regulating the horizontal transport of heat between latitude bands, $I$ is the generalised IR emission for a latitude band. The other terms are the same as the 0DEBM. Specific forms for these functions for the Earth-like model are given in Section 2 A. This model still assumes that the planet is not tidally locked, and that the insolation received is thus an average over a day (diurnally averaged) which is spread over the entire latitude band. The assumption that all latitudes are the same temperature is lifted compared to the 0DEBM.

The 1DEBCM can be derived from the heat equation (see Section 2) and was originally developed by North and Coakley 1979 (NC79) [13] to study the Earth. It was then further applied by Williams and Kasting 1997 (WK97) [14] to study obliquity dependent habitability

and then by Spiegel et al in 2008 (SMS08) [15] and 2009 [16] to study quantify habitability and then study obliquity dependent habitability. Spiegel's work was furthered by Dressing et al 2010 (Dressing10) [17] where eccentricity dependent habitability was investigated. This paper investigates the effects of varying semi-major axis and eccentricity on habitability (Sec. 3 A), as well as obliquity dependence of habitability (Sec. 3 B), and the minimum ratio of ocean to land for the planet to prevent ice-albedo-feedback (Sec. 3 C).

An aspect of the 1DEBCM which is not present in the 0DEBM is ice-albedo-feedback (IAF). It is not present in the 0DEBM because the albedo is constant and the model is not dynamic.

In the 1DEBCM, albedo is a function of temperature where lower temperatures have high albedo and high temperatures have low albedo. If temperature decreases, more ice forms thus albedo increases. This increased albedo means more insolation is reflected, thus the model has even less input heat and so cools further and forms more ice.

Thus, IAF is positive feedback loop between ice formation and albedo which can result in a 'snowball' model which is entirely covered in ice. The susceptibility of the model to IAF can be estimated using the thermal timescale,

$$\tau = \frac{C\Delta T}{I}, \tag{3}$$

which is the energy change in the model divided by the speed of removal of that heat via IR emission. This definition suggests that a larger heat capacity requires a longer time period to change, thus should be less susceptible to IAF.

This is reflected in Sec. 3 C where ocean fraction (thus heat capacity) in the model is varied, and it is found that low ocean fraction (low heat capacity) is much more susceptible to IAF due to the smaller thermal timescale. Two main sources of reduced temperatures are investigated. The first source is eccentricity, where IAF can happen if the planet spends a long time away from the star and cools to a snowball state. The second is obliquity, where IAF can freeze the pole which is facing away from the Sun and then reflect enough light when facing the Sun to allow the entire model to fall into a snowball state.

It is found that obliquity requires higher minimum ocean fraction than eccentricity to avoid IAF and falling into a snowball state, thus is a more powerful constraint on the habitability if the ocean fraction of an exoplanet is known. The disadvantage of this is the eccentricity of the orbit is much easier to observe than the obliquity of the planet relative to the star it orbits.

The 1DEBCM must be validated against known data. To do this a similar process to the one WK97 use to calibrate their model is followed. NC79 used data from various sources and developed a model using Legendre polynomials for latitude variation and sine and cosine functions for time variation. The first 3 terms of the global temperature model are given in their eqn. (4) as

$$T(\lambda, t)[^\circ\mathrm{C}] = 14.2 + 15.5\cos(\omega t + \phi)P_1(\sin\lambda) - 30.2P_2(\sin(\lambda)), \tag{4}$$

where $P_i$ is the $i^{\text{th}}$ Legendre polynomial. Taking the time-average of this function over a year period gives

$$\begin{aligned} T(\lambda)[\mathrm{K}] &= 14.2 + 273 - 30.2(3\sin^2(\lambda) - 1)/2 \\ &= 302.3 - 45.3\sin^2(\lambda), \end{aligned} \tag{5}$$

where the temperature has been converted to Kelvin, and the second Legendre polynomial is expanded as $P_2(x) = (3x^2 - 1)/2$. The average of $\cos(\omega t + \phi)$ over a period $T = 2\pi/\omega$ is 0, so the first Legendre polynomial is not needed. This time-averaged model is then used to fix the diffusion $D$ for the model in Section 2 A.

### C. Habitability

Once the model has been run for a particular set of variables, lots of temperature data for time and latitude must then be processed to evaluate the habitability of the model.

The two habitability functions used in this paper are Liquid Water Requirement (LWR) and Human Compatible (HC). LWR is the more familiar of the two where a temperature between the melting point and boiling point of water is habitable, functionally given as

$$H_{\text{LWR}}(T) = \begin{cases} 1 & 0°\text{C} \leq T \leq 100°\text{C} \\ 0 & \text{Otherwise.} \end{cases} \tag{6}$$

Alternatively, the HC habitability is defined with a smaller range of values,

$$H_{\text{HC}}(T) = \begin{cases} 1 & 0°\text{C} \leq T \leq 30°\text{C} \\ 0 & \text{Otherwise,} \end{cases} \tag{7}$$

with the additional stipulation that if a latitude band experiences a temperature greater than $40°$C or less than $-10°$C then the band is considered uninhabitable for all time. The motivation for this temperature range and restriction of extreme temperatures comes from the ability for humans to self regulate their internal temperature. The typical temperature used to assess human survivability is a wet bulb temperature of $T_w = 30°$C. However, this value can underestimate the onset of hyperthermia and overestimate lethality [18]. This motivates the underestimate of habitability decreasing at $30°$C and being lethal at the higher $40°$C. The minimum temperature is simply a symmetry of the maximum case, and is less important due to cold places staying cold due to IAF.

SMS08 quantifies habitability in 3 main ways. The first is the time-averaged habitability, $f_{\text{time}}$, which is given in their eqn. (6) as

$$f_{\text{time}}(q, \lambda) = \frac{1}{P} \int_0^P H(q, \lambda, t) dt, \tag{8}$$

where $P$ is the length of the year for the model in question and $H(q, \lambda, t)$ is a habitability function; 1 if the temperature is habitable, 0 if not. The second is the area-weighted habitability, $f_{\text{area}}$, which is given in their eqn. (7) as

$$f_{\text{area}}(q, t) = \frac{1}{2} \int_{-\pi/2}^{\pi/2} H(q, \lambda, t) \cos(\lambda) d\lambda, \tag{9}$$

where the area weighting occurs as each latitude band has unequal area. Finally, the combination of these two measures results in the total habitability, $f_{\text{total}}$, given in their eqn. (8) as

$$f_{\text{total}}(q) = \frac{1}{2P} \int_{-\pi/2}^{\pi/2} \int_0^P H(q, \lambda, t) dt \cos(\lambda) d\lambda, \tag{10}$$

where in all three cases the semi-major axis $a$ has been replaced by a generalised parameter (or set of parameters) $q$. This paper uses the discrete form of these equations in Section 2 C in order to both quantify when a model has reached a stable average (i.e. equilibrium) temperature and for quantifying the habitability of a model which varies in time and latitude.

### D. Modifications for Exomoons

In this paper the moon is an Earth-sized moon and the planet is a Jupiter-sized gas giant. In our own solar system there are no moons which come close the size of the Earth, which presents the question: do Earth-sized exomoons exist? The answer is in two parts. First, mass $m > 0.12 M_{\text{Earth}}$ and a strong magnetic field [19] would be required for a "substantial and long-lived atmosphere", thus the exomoons must be high mass. Second, mechanisms such as binary capture [20] can allow for high mass moons where the usual accretion models, such as those that formed the moons seen in the outer solar system, do not.

In order to investigate exomoons the 1DEBCM must be modified to include three heat sources and a reduction to insolation.

In section 4 A eclipsing is investigated and quantified into an eclipsing fraction $\epsilon$. This eclipsing fraction is added to the model as a reduction to the insolation,

$$S(1-A) \to S(1-A)(1-\epsilon), \tag{11}$$

In section 4 B the flux received from the moon due to light from the sun being reflected by the gas giant as well as the emission of light from the gas giant are quantified and added to the model as $F_{\text{ref}}$ and $F_{\text{emiss}}$ respectively. The reflected light from the gas giant is supposed to be from the light not absorbed by the gas giant, which is just the incident light from the sun times the albedo of the gas giant. The emission of the light from the gas giant is then emission of a blackbody in equilibrium given by the 0DEBM. The moon model assumes that the gas giant has radiated all of its heat of formation and thus is in thermal equilibrium with the sun. This is not the case for Jupiter in our own solar system, which the model bases the gas giant after [21], but the additional heat is small.

In section 4 C the tidal heating of the moon due to its elliptical orbit around the gas giant is quantified. Tidal heating equations are described in detail for the specific case of Io in [22, 23] and for general exoplanets in [24, 25]. The general equation for tidal heating is given by

$$F_{\text{th}} = -\frac{21}{8\pi}\text{Im}(k_2)\frac{G^{3/2}M_{\text{gas}}^{5/2}R_{\text{moon}}^{3}e_{\text{moon}}^{2}}{a_{\text{moon}}^{15/2}}, \tag{12}$$

where the mass, radius, eccentricity, and semi-major axis of the subscripted body are given by $M$, $R$, $e$, and $a$ respectively. Specific values for $-\text{Im}(k_2)$ are derived from different rheologies and material compositions of the moon. In this paper the Maxwell rheology from Henning et al [26] is used as well as the material compositions from Dobos and Turner [24].

Thus, the moon model is, with all modifications made, given by

$$\begin{aligned} C\frac{\partial T}{\partial t} =& D\left[\frac{\partial^2 T}{\partial \lambda^2} - \tan\lambda\frac{\partial T}{\partial \lambda}\right] - I(T) \\ &+ F_{\text{ref}} + F_{\text{emiss}} + F_{\text{th}} + S(1-A_{\text{moon}})(1-\epsilon). \end{aligned} \tag{13}$$

| Semi-major axis $a$, au | Eccentricity $e$ | Obliquity $\delta$, deg | No. spatial nodes $S$ | Timestep $\Delta t$, days | Land fraction type |
|---|---|---|---|---|---|
| 1 | 0.0167 | 23.5 | 61 | 1 | Uniform 70% Ocean |

**TABLE I:** A summary of the default parameters for the Earth-like model. A 'Uniform' land fraction indicates that the model has the same ratio of land to ocean across the entire planet. The odd number of spatial nodes means there is a true equator with $\lambda = 0$ as well as poles with $\lambda = \pm 90^\circ$

With this moon model the habitable zones investigated in Sec. 3 can be revisited to see how they are affected by the changes (Sec. 4 D). New habitable zones also emerge depending on the moon's parameters. The semi-major axis and eccentricity of the moon's orbit are investigated in Sec. 4 E.

## 2. 1-D ENERGY BALANCE CLIMATE MODEL

The 1DEBCM can be derived from the standard heat equation given by

$$\frac{\partial T}{\partial t} = \alpha \nabla^2 T, \tag{14}$$

where $T(t, r, \theta, \phi)$ is the temperature at time $t$, radius $r$, co-latitude $\theta$, and longitude $\phi$. The constant $\alpha$ is related to the heat capacity and diffusion rate of the system. Expanding the Laplacian in spherical coordinates the equation becomes

$$\frac{\partial T}{\partial t} = \alpha \left[ \frac{1}{r} \frac{\partial^2}{\partial r^2}(rT) + \frac{1}{r^2 \sin\theta} \frac{\partial}{\partial \theta} \left( \sin\theta \frac{\partial T}{\partial \theta} \right) + \frac{1}{r^2 \sin^2\theta} \frac{\partial^2 T}{\partial \theta^2} \right]. \tag{15}$$

The 1DEBCM is arrived at by first letting $T(t, r, \theta, \phi) = T(t, \lambda)$, with latitude $\lambda = \pi - \theta$. Thus, the equation simplifies to

$$\begin{aligned} \frac{\partial T}{\partial t} &= \frac{\alpha}{r^2 \sin\theta} \frac{\partial}{\partial \theta} \left( \sin\theta \frac{\partial T}{\partial \theta} \right) \\ &= \frac{\alpha}{r^2} \left( \frac{\partial^2 T}{\partial \lambda^2} - \tan\lambda \frac{\partial T}{\partial \lambda} \right). \end{aligned} \tag{16}$$

The original equation can be recovered by defining $\alpha / r^2 \equiv D/C$ for diffusion constant $D$ and heat capacity $C$. Then adding incoming solar radiation $S$ (insolation), which is reduced by planetary albedo $A$, and outgoing IR-emission $I$ to the PDE. Thus, the original form of the 1DEBCM in eqn. (2) is recovered.

### A. Earth-like Model Functions

In order to investigate the Earth and Earth-like planets, the parameters and functions which define the Earth must be established. In this analysis the forms of the Earth-like functions are taken from WK97, and the Earth-like model is compared against a model derived from NC79.

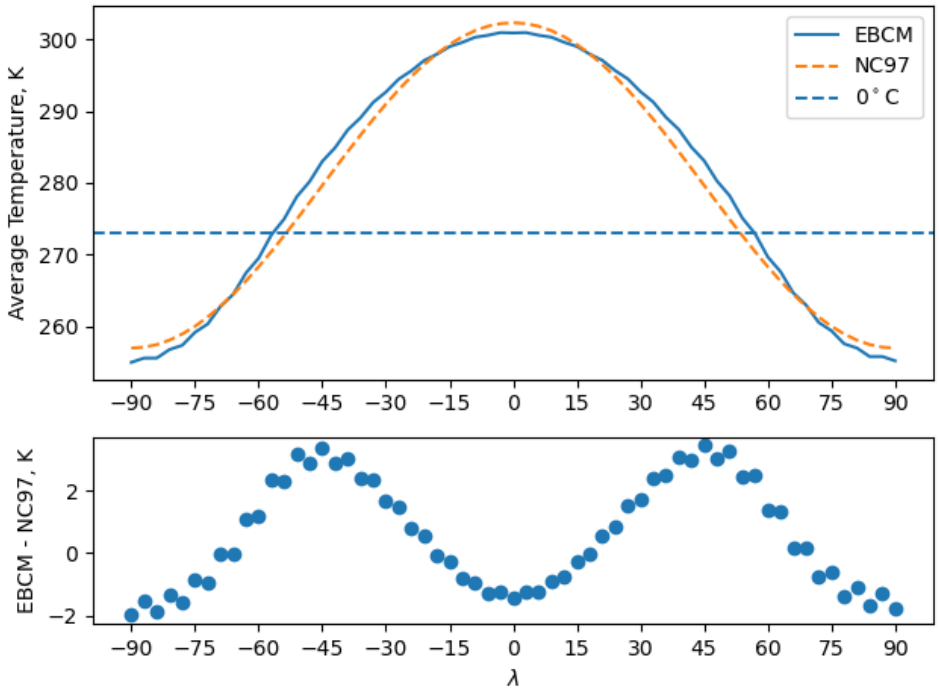


**FIG. 1:** The 10-year-averaged temperature distribution of the Earth-like model given in I. Overlaid on the fit is the time averaged Earth model from North and Coakley's 1979 paper [13]. The diffusion parameter $D_0$ in eqn. (17) was varied to give the best agreement between the two models. The value found to work best is $D_0 = 0.56$ Wm$^{-2}$K$^{-1}$.

The diffusion constant, $D$, varies with orbital and atmospheric parameters as

$$\frac{D}{D_0} = \frac{p}{p_0}\frac{c_p}{c_{p,0}}\left(\frac{m}{28}\right)^{-2}\left(\frac{\Omega}{1\text{ day}^{-1}}\right)^{-2}, \tag{17}$$

where $D_0 = 0.56$ Wm$^{-2}$K$^{-1}$ is from fitting to eqn. (5) as shown in Fig. 1. The atmospheric pressure, $p$, is relative to one atmosphere of pressure, $p_0 = 101$ kPa. The heat capacity, $c_p$, of the atmosphere is relative to $c_{p,0} = 1 \times 10^3$ g$^{-1}$K$^{-1}$, which is the heat capacity of nitrogen gas. Average mass of particles in the atmosphere is given by $m$ and is relative to the nitrogen molecule. Rotation rate of the planet, $\Omega$, is relative to Earth's 1 rotation per day. These parameters can be extended to be time variable, such as having $CO_2$ emissions increase pressure, change heat capacity, and change mass of particles. However, this is beyond the scope of this paper.

Heat capacity, $C(\lambda, T)$, varies with latitude through the ocean-land fraction, $f_o(\lambda)$, and with temperature through the ice-ocean fraction, $f_i(T)$, as

$$C(\lambda, T) = (1 - f_o(\lambda))C_{\text{land}} + f_o(\lambda)((1 - f_i(T))C_{\text{ocean}} + f_i(T)C_{\text{ice}}(T)), \tag{18}$$

Where $C_{\text{land}} = 5.25 \times 10^6$ Jm$^{-2}$K$^{-1}$ and $C_{\text{ocean}} = 40 \times C_{\text{land}}$ are constant, and

$$C_{\text{ice}}(T) = \begin{cases} 9.2C_{\text{land}} & T \geq 263\text{K} \\ 2.0C_{\text{land}} & T < 263\text{K}, \end{cases} \tag{19}$$

which encapsulates the additional energy requirements of the heat of fusion, and expects that the water would be entirely frozen below $-10$°C. The ratio of ocean to land for the Earth is

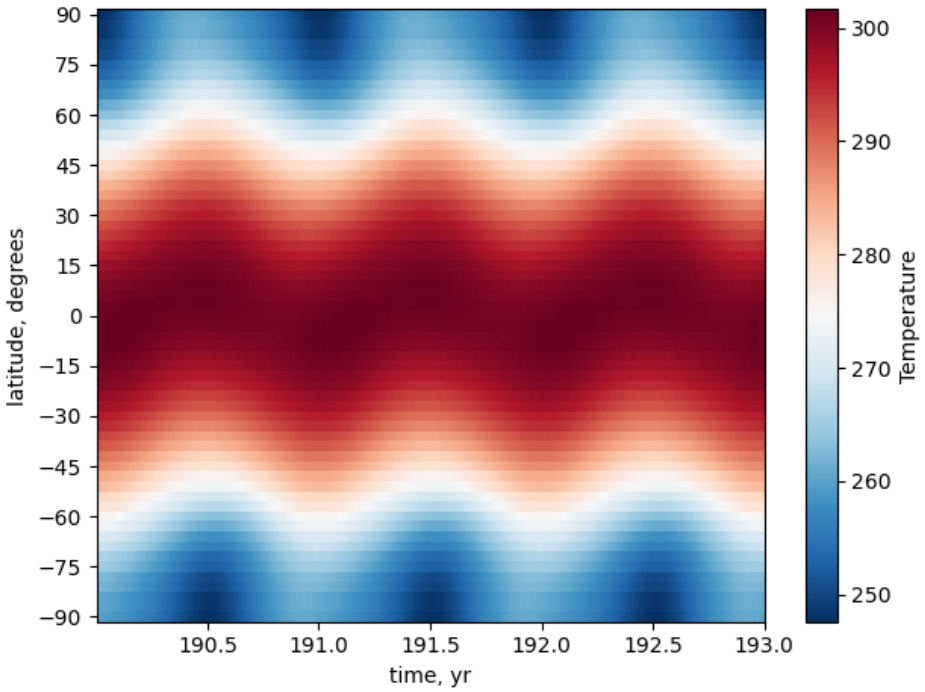


**FIG. 2:** The temperature distribution for the Earth model with parameters given in Table I. The time range is for 2 years starting in the 190th year of evolution. There is clear periodicity of the seasons in the model, indicating that the model has reached a stable equilbrium.

70% ocean to 30% land. This model assumes this ratio is uniform and constant across the entire planet, thus $f_o = 0.7$. This is a simplification as the Earth has an uneven distribution of land and ocean, with most of the land in the Northern Hemisphere.

With definitions of diffusion and heat capacity, the time step and latitude step which are numerically stable can be calculated. To do this the EBCM is investigated with a plane wave solution and boundaries on the time step and latitude step are found. The explicit calculation of this is shown in appx. A, with the result that, for constant diffusion and time step, a lower heat capacity requires a larger latitude step. The default values for the model are then taken as a time step of $\Delta t = 1$ day and $S = 61$ latitude nodes ($\Delta\lambda = 3^\circ$ separation). These parameters give good resolution while being completely numerically stable. For planets with $f_o = 0$ (see Sec. 3 C) a lower value of $S = 31$ is chosen as it is stable for the land-only heat capacity value.

WK97 provides three sets of IR-emission and Albedo functions. Following the example of SMS08 and Dressing10, the second set of IR and Albedo functions which are given by

$$I(T) = I_2(T) = \frac{\sigma T^4}{1 + 0.5925(T/273\text{K})^3} \tag{20}$$

$$A(T) = A_2(T) = 0.525 - 0.245 \tanh\left(\frac{T - 268\text{K}}{5}\right), \tag{21}$$

are used in all models. This IR-emission is a blackbody radiation term (numerator) damped by the optical thickness of the atmosphere (denominator) which is roughly equivalent to the greenhouse gas effect due to water vapour content in the air. The albedo function is a smooth scaling from low reflectivity of land and forest to high reflectivity due to ice and snow.

The insolation function, $S$, is defined in WK97 as the day averaged incident (based on latitude) radiation from the sun,

$$S(\lambda,t)=\frac{q_0}{\pi}\left(\frac{1\text{ au}}{r(t)}\right)^2(H(t)\sin\lambda\sin\delta(t)+\cos\lambda\cos\delta(t)\sin H(t)), \tag{22}$$

where $q_0 = 1360$ Wm$^{-2}$ is the insolation from the Sun, $r(t)$ is the distance from the Sun, $\cos H(t) = -\tan\lambda\tan\delta(t)$ is the radian half-day length with $0 < H < \pi$, and $\delta(t)$ is the solar declination defined by

$$\sin\delta(t) = -\sin\delta_0\cos(L_s(t)+\pi/2), \tag{23}$$

where $\delta_0$ is the obliquity of the planet and $L_s(t) = \omega t$ is orbital longitude from an orbital angular velocity found by Kepler's laws. It is important to average over a day insolation as the model does not have a longitude dimension, so cannot account for uneven distribution of the insolation, for example in the case of a tidally locked planet.

The distance from the Sun is variable due to eccentricity. For a 2-body system this distance can be calculated through an iterative method as follows

$$r(t) = a(1-e\cos E(t)), \tag{24}$$

where $a$ and $e$ are semi-major axis and eccentricity respectively, and the eccentricity anomaly $E$ is given by iteration

$$\begin{aligned} E_0 &= M \\ E_{i+1} &= E_i + \frac{M+e\sin E_i - E_i}{1-e\cos E_i}, \end{aligned} \tag{25}$$

where $M = 2\pi(t+t_0)/T$ for a temporal offset $t_0$ and period of the orbit $T$. The error in this function increases with higher $e$ but reduces with additional iterations. Three iterations with an eccentricity of $0.9$ gives an error in $E$ of 5% (compared to 100 iterations), which is a good compromise between computation time and accuracy, especially as $e = 0.9$ is the upper bound for eccentricities considered.

The temperature distribution for the Earth model is shown in Fig. 2 for 2 years after 190 years of evolution. There is clear periodicity in the model corresponding clearly with the seasonal variations experienced by the Earth.

### B. Discretisation and Time Evolution

Numerically integrating the EBCM requires the derivatives to be discretised. Spatially the planet can be split into $S$ latitude bands, separated by

$$\Delta\lambda = \frac{\pi^{\text{rad}}}{S-1} = \frac{180^\circ}{S-1}, \tag{26}$$

with spatial indexing of each band from $m = 0, 1, \ldots, S-1$. Similarly, a temporal indexing of $n = 0, 1, \ldots$ is used to discretise time in steps of $\Delta t$. Thus, $T_n^m$ is the temperature at the $m^{\text{th}}$ time step for the $n^{\text{th}}$ latitude band.

The spatial derivatives can then be approximated by the central difference and second order central difference:

$$\frac{\partial T_n^m}{\partial \lambda} = \frac{T_n^{m+1} - T_n^{m-1}}{2\Delta\lambda}, \tag{27}$$

$$\frac{\partial^2 T_n^m}{\partial \lambda^2} = \frac{T_n^{m+2} - 2T_n^m + T_n^{m-2}}{(2\Delta\lambda)^2}, \tag{28}$$

and the temporal derivative can be approximated as a forward difference,

$$\frac{\partial T_n^m}{\partial t} = \frac{T_{n+1}^m - T_n^m}{\Delta t}, \tag{29}$$

with numerical stability analysed in appendix A. Evolving the EBCM is performed by solving eqn. (29) for $T_{n+1}^m$ in terms of the parameter and temperature values at time step $n$.

However, a problem arises at the edges of the model as $m = -2, -1, S, S+1$ are not defined. To fix this the derivatives at $m = 0$ ($m = S - 1$) are discretised as forward then backward (backward then forward) derivatives. By imposing that $\partial T_n^{m=0,S-1}/\partial\lambda = 0$, the second order derivatives then reduce to

$$\frac{\partial^2 T_n^{m=0}}{\partial \lambda^2} = \frac{1}{\Delta\lambda}\left(\frac{\partial T_n^{m=1}}{\partial \lambda} - \frac{\partial T_n^{m=0}}{\partial \lambda}\right) = \frac{T_n^{m=1} - T_n^{m=0}}{(\Delta\lambda)^2} \tag{30}$$

$$\frac{\partial^2 T_n^{m=S-1}}{\partial \lambda^2} = \frac{1}{\Delta\lambda}\left(\frac{\partial T_n^{m=S-1}}{\partial \lambda} - \frac{\partial T_n^{m=S-2}}{\partial \lambda}\right) = \frac{T_n^{m=S-2} - T_n^{m=S-1}}{(\Delta\lambda)^2}. \tag{31}$$

Furthermore, the treatment imposed for the $m = 1$ and $m = S - 2$ second order derivatives is much the same, using central-backward and central-forward derivatives respectively.

### C. Averaging and Habitability

Analysing the data produced requires the use of area-weighted averaging and time averaging from SMS08. The original equations are given as continuous integrals, but are discretised in a similar way to the derivatives in 2 B. Thus, the time averaging, area-weighted averaging, and total averaging are given by

$$Q_{p\to q}^m = \frac{\sum_{n=p}^q Q_n^m \Delta t}{\sum_{n=p}^q \Delta t} = \frac{\sum_{n=p}^q Q_n^m}{t_q - t_p}, \tag{32}$$

$$\bar{Q}_n = \sum_{m=0}^{S-1} Q_n^m F^m = \sum_{m=0}^{S-1} \frac{1}{2} Q_n^m \cos(\lambda_m)\Delta\lambda, \tag{33}$$

$$\bar{Q}_{p\to q} = \frac{\sum_{n=p}^q \sum_{m=0}^{S-1} Q_n^m \cos(\lambda_m)\Delta\lambda}{2(t_q - t_p)}, \tag{34}$$

respectively, with the time averaging happening between a time $t_p$ and $t_q$. These averages can now be used to evaluate if a model has reached an equilibrium temperature and what the average habitability of a planet is.

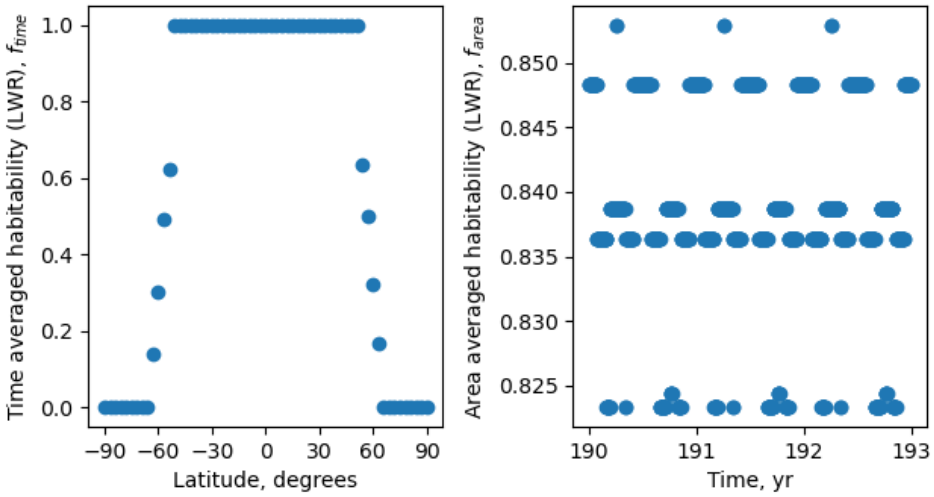


**FIG. 3:** A demonstration of the LWR Habitability function with time averaging, eqn. (32) (left), and area-weighted averaging, eqn. (33) (right). The time averaged habitability is for a 10-year period, and the area-weighted averaged is over the entire planet and is shown for three years.

A model is said to reach an equilibrium temperature when the fractional difference between the average temperature of 2 periods is less than some tolerance $\epsilon$:

$$\left|1 - \frac{\bar{T}_{q\to r}}{\bar{T}_{p\to q}}\right| < \epsilon, \tag{35}$$

for some times $t_r > t_q > t_p$. Typically, the averaging occurs over an orbital period (i.e. local year), so the equilibrium temperature is when there are no significant variations in temperature between two consecutive orbits. The value of $\epsilon$ chosen directly influences how long the model must be run to reach an equilibrium. In most cases a value of $\epsilon = 10^{-3}$ is used and results in equilibrium times of between $20$ and $150$ years depending on model parameters.

In fig. 3 the use of these functions is demonstrated on the temperature data for the Earth (fig. 2). It is processed using the LWR habitability which has then been time averaged with eqn. (32) and area averaged with eqn. (33).

The time-averaged habitability shows how the equator is habitable all year around. The poles are uninhabitable year round. Between $65°$ to $45°$ the habitability decreases linearly, representative of the variability of the frost line where latitudes close to the pole are very rarely habitable and latitudes in this range closer to the equator are very rarely uninhabitable.

The area averaged habitability changes in steps as each discrete latitude band becomes habitable or uninhabitable. It is periodic, but difficult to predict within each year.

The total averaged habitability is $H_{\text{Earth}} = 0.84$, meaning that the Earth is, when using LWR, $84\%$ habitable. When using HC habitability this value is slightly reduced but the same to two significant figures.

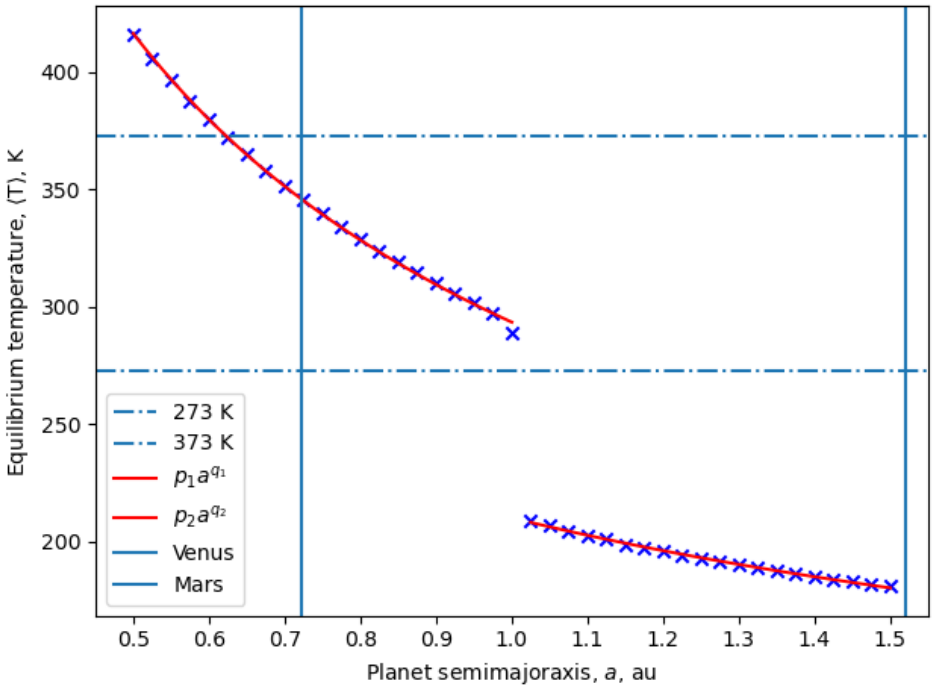


**FIG. 4:** A plot of the equilibrium temperature of the planet when varying its semi-major axis at constant eccentricity of $e = 0.0167$. Overlaid on the plot are two curves which are fitted to the data by a least squares regression. The form of the curve is $\langle T \rangle = p_i a^{q_i}$. Also shown are the orbits of Venus and Mars to highlight the range of values considered.

## 3. INVESTIGATING EARTH-LIKE EXOPLANETS

### A. Varying Semi-major Axis and Eccentricity

General temperature relations for a planet can be found from the 0DEBM. Time averaged insolation of a planet in an elliptical orbit is given by

$$S = \langle F \rangle = \frac{q_0}{a^2\sqrt{1-e^2}}, \tag{36}$$

where $q_0 = L_{\text{Sun}}/4\pi a_{\text{Earth}}^2 \approx 1360$ Wm$^{-2}$ is the bolometric solar flux for Earth, $a$ and $e$ are the semi-major axis and eccentricity respectively of the planet [28].

By substituting this relation into equation (1), the temperature of a planet can be related to semi-major axis and eccentricity through

$$T \propto a^{-\frac{1}{2}}(1-e^2)^{-\frac{1}{8}}, \tag{37}$$

with proportionality constant $(q_0(1-A)/4\sigma)^{1/4} = 255$ K for an Earth-like albedo of 0.3.

The validity of this proportionality can be investigated in terms of the semi-major axis by keeping $e = 0.0167$ constant and varying $a$ from just outside Mercury's orbit at $0.5$ au to Mars' orbit at $1.5$ au. As seen in Figure 4 there are three main zones of interest to consider.

The first zone with $a < 0.65$ au has temperatures too high to sustain liquid water due to being too close to the Sun. The second zone with $0.65 < a < 1$ au is much more temperate,

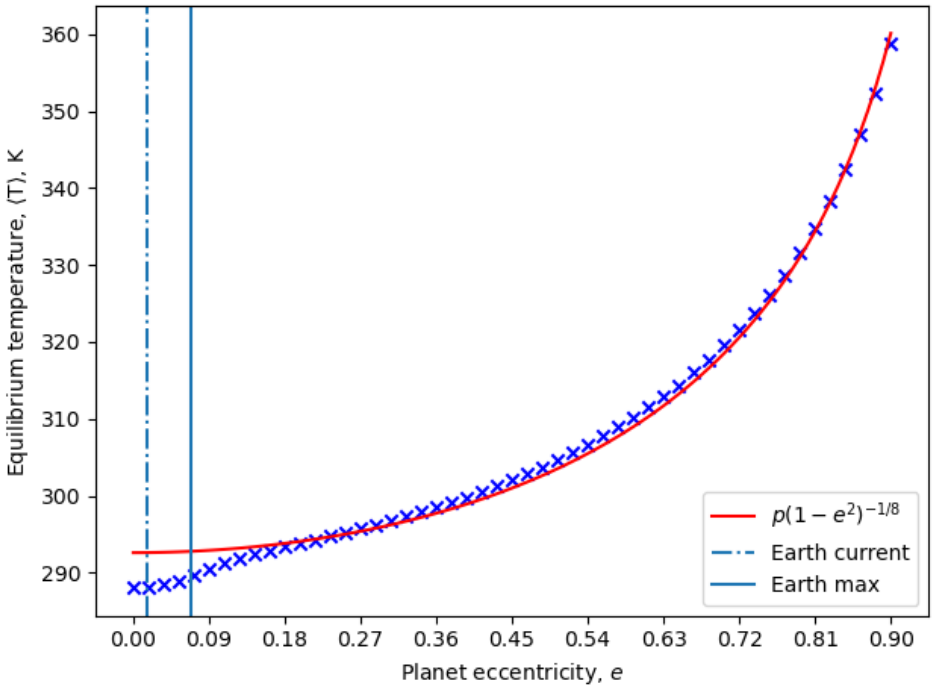


**FIG. 5:** A plot of the equilibrium temperature of the planet when varying its eccentricity at constant semi-major axis of $a = 1$ au. Overlaid on the plot is a curve which is fitted to the data by a least squares regression. The form of the curve is $\langle T \rangle = p(1-e^2)^{-1/8}$. Also shown are the current and maximum theoretical value of Earth's eccentricity [27]. The minimum value is 0. There is a dip from the model at lower eccentricities due to IAF forming polar icecaps.

and is able to sustain liquid water on the planet's surface. Both the first and second zones are described by $\langle T \rangle = p_1 a^{q_1}$ with $p_1 = 293.5 \pm 0.4$ and $q_1 = -0.505 \pm 0.004$. $q_1$ is very close to the expected $-0.5$ power law seen in eqn. (37). However, the value of $p_1$ is 38 K higher than the expected proportionality, most likely due to the additional greenhouse effect present in the 1D model.

The third zone with $a > 1$ au is a sudden departure from this expected power law, with $p_2 = 210.2 \pm 0.2$ and $q_2 = -0.378 \pm 0.003$. This is due to IAF which works as follows. As the planet cools, ice forms with a higher albedo than the land or ocean. This higher albedo means more light is reflected, thus the planet absorbs less heat, so cools more. This cycle continues until the planet reaches a much colder equilibrium than is expected by a fixed albedo method. At 1 au the planet is on a tipping point in terms of this feedback loop, as seen by the temperature being slightly lower than expected by eqn. (37). This, along with the following analysis of eccentricity and obliquity, help show why the Earth has had many ice ages in the past [29].

Alternatively, $a$ can be fixed at 1 au and the eccentricity can be varied from a perfect circle, $e = 0$, to a very eccentric ellipse, $e = 0.9$. Beyond $e > 0.9$ the iteration to find orbital distance converges much less quickly so becomes intractable. Additionally, planets in extreme orbits with $e > 0.9$ would be extremely unstable and most likely would not be able to retain an atmosphere due to extreme temperatures.

Varying the eccentricity is similar to varying the semi-major axis. There are two main zones

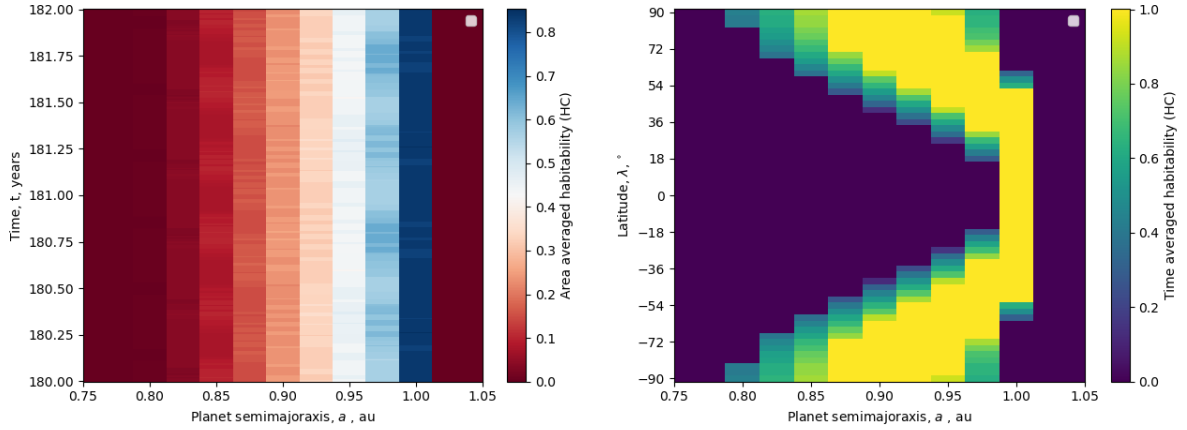


**FIG. 6:** Left: A heatmap for area-averaged HC habitability for a 2 years on the y-axis and planet semi-major axis between $0.75$ and $1.05$ au on the x-axis. The planet is never $100\%$ habitable, reaching a maximum of $85\%$ when at the Earth-like $1$ au. Right: A heatmap for the 10-year time-averaged HC habitability for each latitude band on the y-axis and the same planet semi-major axis values on the x-axis. In this case some latitude bands do reach $100\%$ habitability.

of interest in Figure 5 where the eccentricity of the planet is varied.

The zone with $e > 0.2$ follows the relationship well, and the globally averaged temperature doesn't exceed the boiling point of water. On the other hand, the zone with $e < 0.2$ is up to $5$ K lower than the relationship. This dip is again due to IAF. High eccentricities mean the planet gathers and stores enough thermal energy when close to the Sun to prevent polar ice caps from forming even when further away from the Sun. Lower eccentricities allow for polar ice caps to form which then significantly lower the global temperature.

As seen from the vertical lines in Fig. 5, the Earth has moved in this lower eccentricity region for its entire history, suggesting that the presence of the polar caps has been reasonably constant for the recent past.

In Fig. 6 the semi-major axis of the planet is varied between just outside Mercury's orbit and Mars' orbit at constant eccentricity in order to investigate how HC habitability changes. The area-averaged habitability shows slight variations in habitability over time. This variation occurs for two main reasons: the growth and recession of the polar icecaps and equatorial desert. This growth and recession is shown in the time-averaged habitability where polar and equatorial regions have habitabilities between 0 and 1, indicating they are partially habitable over time.

As $a$ decreases from $1$ au, the planet experiences higher insolation. This higher insolation gives rise to higher temperatures across the planet. This melts the poles which are otherwise frozen, and causes the already hot equator to become too hot to sustain life.

Slightly increasing $a$ from $1$ au, the planet experiences a sharp drop in temperature. This is due to IAF where a small temperature decrease allows the icecaps to grow, and further decrease insolation until the entire planet is covered in ice.

In this case the HC habitability means that an Earth-like planet would not be habitable at the orbits of our closest neighbours, Venus and Mars.

Similarly, Fig. 7 shows the effects on habitability when the eccentricity of the planet is varied from $0$ to $0.9$. At low eccentricities, such as those the Earth has experienced in its history, there

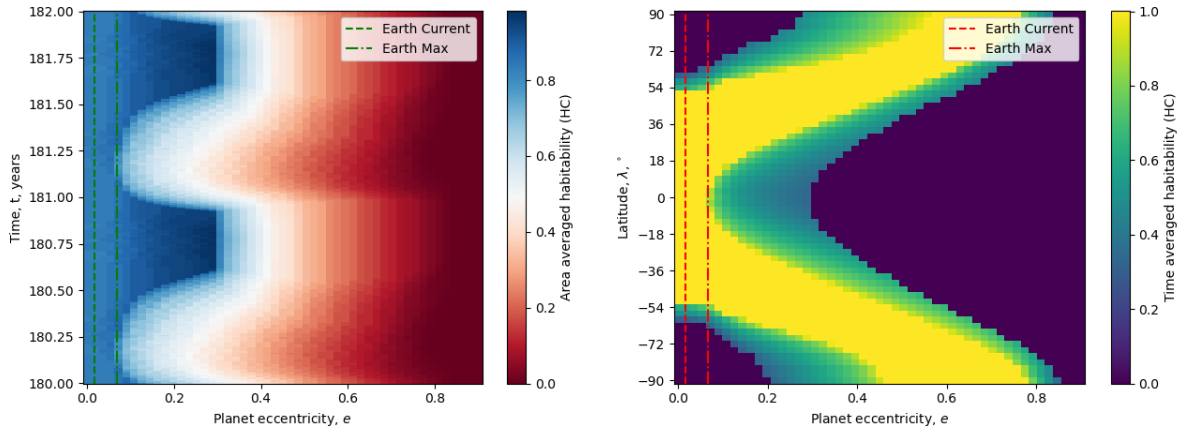


**FIG. 7:** Left: A heatmap for area-averaged HC habitability for a 2 years on the y-axis and planet eccentricity between 0 and 0.9 on the x-axis. The planet is never 100% habitable, reaching a maximum of 85%. Right: A heatmap for the 10-year time-averaged HC habitability for each latitude band on the y-axis and the same planet eccentricity values on the x-axis. As eccentricity increases the habitable zones of the planet move outwards towards the poles because they are less directly insolated.

is little variation both in area- and time-averaged habitabilities.

Increasing eccentricity results in more seasonality. For example for $e = 0.2$ the planet has an area averaged habitability which starts at 0.5, increases to 0.85, then decreases again at the turn of the year. This is because the planet's temperature is too hot in the first half of the year near the Sun, and is temperate all over the planet for the other half of the year as the planet is allowed to cool away from the Sun. However, for eccentricities $e > 0.3$ the hot spike as the planet is close to the Sun exceeds the maximum limit and latitude bands at the equator are considered fully uninhabitable. This results in a sizeable decrease in habitability for the other half of the year when the planet is cooling.

At extreme values of eccentricity, only the poles stay cool enough year round to harbour life. However, this represents a small fraction of the surface area of the planet. At eccentricities above $e > 0.8$ the poles become too hot for life at certain parts of the year, and eventually are totally uninhabitable.

So far the semi-major axis and eccentricity have been varied independently to investigate effects on the time and area habitabilities. Varying both together can illuminate the habitability parameter space for orbits in exoplanet systems. This is shown in Fig. 8 where the semi-major axis and eccentricity of a planet are varied together. The top graph is a heatmap for the equilibrium temperature of the planet, and the bottom graphs are the processing of the temperature data using the LWR habitability and HC habitability. The temperature heatmap highlights the drop-off in temperature when IAF starts and the planet falls into a snowball. There exist some above freezing temperatures for high eccentricity and high semi-major axis, likely due to the planets unfreezing when close the Sun, and refreezing when further away.

Both habitabilities show similar shapes but different widths which is reflective of HC being more restrictive in temperature range than LWR. The difference in the habitabilities is shown at high eccentricity. The LWR habitability suggests that there is a wide range of semi-major axis values where liquid water exists on the surface of the planet year-round at high eccentrici-

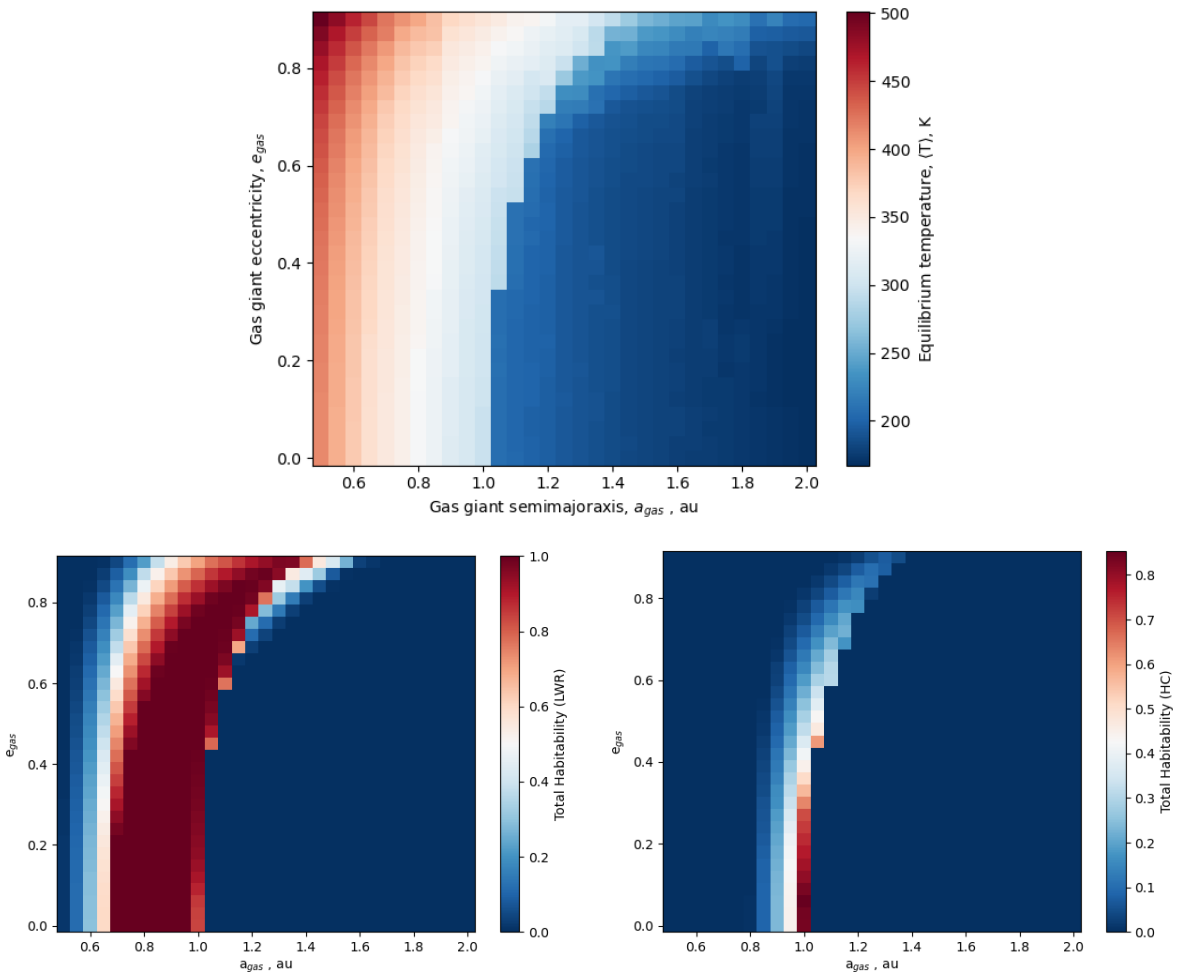


**FIG. 8:** Top: Varying the semi-major axis and eccentricity of the gas giant to produce a heat map for the equilibrium temperature of the planet. Left: Processing of the temperature data with eqn. (6). Right: Processing of the temperature data with eqn. (7).

ties. Alternatively, the HC habitability indicates that these high eccentricities have extremes of temperature which are not compatible with life, thus the actual habitability is likely lower.

### B. Varying Obliquity

The obliquity of the planet's spin can be varied to see how the habitability profile changes. Due to the uniform nature of the planet there is a symmetry about $\delta = 90°$. Because of this symmetry only values between $0°$ and $90°$ need to be considered.

Varying obliquity is shown in Fig. 9. There are three main areas to consider:

- Low obliquity $(0° - 20°)$ where the planet directly presents its equator to the Sun for the majority of its orbit.

- Medium obliquity $(20° - 50°)$ where the planet presents both the equator and poles to the Sun in roughly equal amounts.

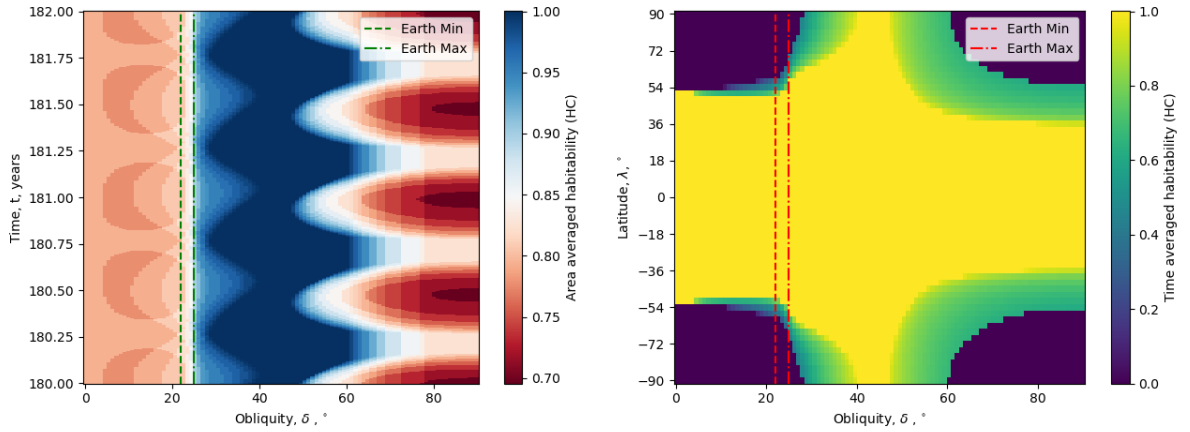


**FIG. 9:** Left: The area-averaged human habitability for a 2-year period after 150 years of simulation. The habitability varies between 70% and 100%, with the highest habitabilities being between 20°and 50°At lower obliquities polar ice caps form reducing the area habitability. Right: The 10 year time-averaged human habitability for each latitude band. Habitability at the equator of this planet is usually totally habitable all year around.

- High obliquity ($50° - 90°$) where the planet cycles between presenting a pole to the Sun and presenting the equator (sideways) to the Sun.

For low obliquities there are small habitability variations. These variations are due to the permanent icecaps growing and shrinking. As the cap grows more latitude bands are below freezing so area-averaged habitability decreases. As the cap shrinks the opposite occurs, and area-averaged habitability increases. At especially low obliquities the shrinking and growing is smaller than the width of a latitude band, so the habitability is constant.

At medium obliquities the icecaps are insolated directly enough to be melted. The lower end of this range has the icecaps reform for the portion of the year that they are facing away from the Sun, and then melt in the portion of the year when facing toward the Sun. This results in some seasonal habitability. In the middle of this range the poles are melted for the entire year. This suggests an optimal range for obliquity where the insolation is spread out evenly across the planet, allowing for the entire surface to be temperate (and thus habitable) for all time.

At very high obliquities each pole is either directly insolated or in shadow for long periods of time, so experience extreme temperatures. The pole which is being directly insolated becomes very hot and can exceed the maximum temperature which sets the habitability of the latitude band to 0 for all time. Conversely, the pole which is in constant shadow quickly cools and freezes over. This exceeds the minimum temperature for habitability. Between the poles is a steep temperature gradient from hot to cold pole. This gives rise to the 80% habitability regions between dark spots where the habitability is at its highest for large obliquity.

As the planet moves in the orbit the equator is directly insolated and both poles are only partially insolated. The equator has a much larger area so can distribute this extra heat better so exceeds the habitable limit but not the maximum temperature. The poles at this time are able to melt or cool as appropriate. While the temperatures they reach at this time may be suitable for life, they exceeded the maximum limit so are still considered uninhabitable. The overall effect are seen in the darker 70% habitable regions where the poles and equator both have reduced

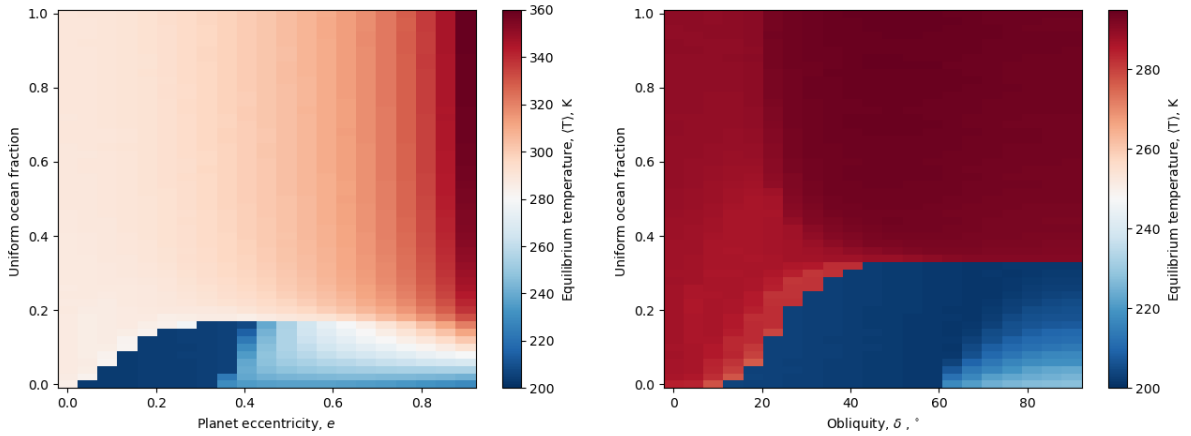


**FIG. 10:** A heatmap for equilibrium temperature when varying ocean fraction with eccentricity (Left) and obliquity (Right). The two main regions in both graphs are the warm temperatures with higher ocean fraction and much colder temperatures with lower ocean fractions. While both temperature scales start at 200 K, the eccentricity graph reaches 360 K whereas the obliquity graph reaches 295 K.

habitability.

Most planets have obliquities which can vary through this entire range of values. The Earth is an exception to this. The Moon stabilises the Earth's obliquity to vary between $22°$ and $25°$ with a current value of $23.5°$ (decreasing). In this range the habitability is fairly constant.

### C. Varying Ocean Fraction with Eccentricity and Obliquity

The snowball state produced by IAF has been seen when varying semi-major axis (Figs. 4 and 6) and partially when varying eccentricity (Fig. 5). A variable which influences susceptibility to IAF is the ocean fraction.

The thermal timescale (eqn. (3)) means that ocean, which has a higher heat capacity than land, has a larger thermal inertia. Larger thermal inertia means the ocean on the planet helps to reduce temperature variations which the planet experiences. Thus, it is expected that planets with low ocean fraction will be susceptible to IAF in shorter timescales or with less forcing than high ocean fraction planets. The main orbital variables influencing this forcing are the eccentricity and obliquity.

In an eccentric orbit the insolation decreases as the planet moves away from the Sun. This reduced insolation causes a lower temperature for a portion of the year. If the temperature is reduced enough, IAF can kick in and cause the planet to fall into a snowball state that it cannot recover from.

Obliquity can also cause snowball states. Obliquity for the Earth means seasons, where winter occurs in a hemisphere when that hemisphere points away the Sun because it is less directly insolated. The severity of this winter depends on how much of the pole is in permanent shadow and how long the winter lasts. Permanent shadow is influenced by the obliquity of the planet, and the length of the winter depends on the period of the orbit. Varying obliquity will allow for the investigation of the permanent shadow effect.

To investigate these expectations the ocean fraction of the model is varied in Fig. 10. In the

left plot ocean fraction is varied against eccentricity with zero obliquity, and in the right plot ocean fraction is varied against obliquity with zero eccentricity.

We see that for eccentricity there as a minimum ocean fraction which increases with eccentricity until a maximum at $e = 0.3$ of $f_{\text{ocean}} = 20\%$. Using the average temperature when not in equilibrium ($T = 300$ K) and assuming that the planet must drop in temperature to be at least below freezing ($\Delta T = 30$ K) then the thermal timescale for this model at minimum ocean fraction is $\tau = 5.2 \times 10^6$s $\approx$ 2months. This means that this model is susceptible to IAF on the timescale of 2 months when at minimum ocean fraction, with shorter time scales at lower ocean fractions. The value is approximate as higher eccentricities increase the maximum temperature, thus increasing IR emission, but also increasing the required change in temperature. At $e = 0$ there is no temperature variation, so the model cannot fall into a snowball state. As eccentricity increases the minimum ocean fraction, thus minimum thermal inertia, required to prevent a fall into a snowball state increases as expected. Unexpected is the region after $e > 0.4$.

At much higher eccentricities and low ocean fraction the planet moves further from the Sun so falls into a snowball state more easily. It can also move closer to the Sun which then increases the insolation. This insolation can be higher enough to allow the planet to melt and leave the snowball state. The combination of these two effects is that the planet is very hot half of the year and frozen for the other half of the year, with an average temperature which is habitable.

The habitability of this sort of planet is difficult to quantify. Humans have survived ice ages in the past by burning fuels and sheltering in caves, to give just two examples. We are yet to see if human life will survive extreme heat.

Similarly, when varying obliquity the minimum ocean fraction starts at 0 and increases until a maximum of $36\%$ at roughly $\delta = 45°$. For $0° < \delta < 10°$ the planet does not fall into a snowball state as the permanent shadow region is not large enough to cause runaway IAF. The thermal timescale for this obliquity case is roughly twice the eccentricity case, $\tau = 3.9$ months. This means that the IAF from obliquity acts over a much longer timescale than the eccentricity case, thus requires that the planet has a higher thermal inertia in the form of oceans to prevent it.

For Earth-like obliquities (between $22°$ and $25°$) the planet is susceptible to a snowball state only if the planet has ocean fraction less than roughly $15\%$.

At very high obliquities (and low ocean fractions) the pole which faces the Sun can be melted. This is because low ocean fraction has low heat capacity, so the heat input from the direct insolation to the polar region can raise the temperature of the region very easily. This is very localised to the polar region and so only slightly raises the average temperature of the planet.

The minimum ocean fraction for the obliquity case is much larger than the eccentricity case. This is indicative that the temperature variations due to obliquity are much larger than variations due to eccentricity. This is likely due to the obliquity having a more localised effect on the polar regions of the planet as opposed to eccentricity's planetwide effect.

Both variables cause the planet to be susceptible to IAF, and both cause full or partial recovery from snowball at extreme values. For eccentricity the minimum ocean fraction varies approximately quadratically with eccentricity until $e = 0.4$ where the eccentricity is high enough to melt the induced snowball meaning the time averaged temperature increases. The minimum ocean fraction in the obliquity case varies with an 'S' shape and levels out after $\delta = 45°$ to

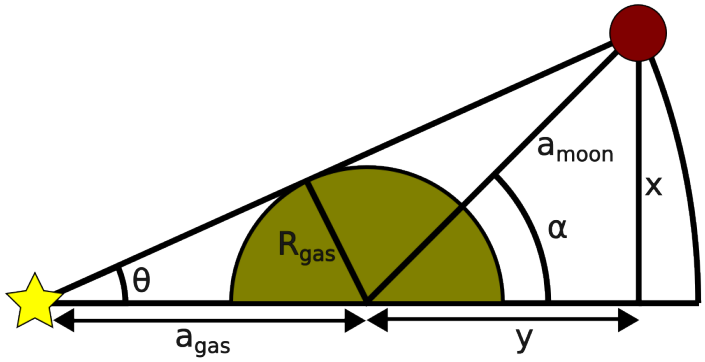


**FIG. 11:** A diagram of a gas giant (middle green hemisphere) in orbit around a star (left yellow shape) at a distance $a_{\text{gas}}$, and a moon (top right maroon circle) in orbit of the planet at a distance $a_{\text{moon}}$. The planet has radius $R_{\text{gas}}$. The angle $\theta$ corresponds to half the angular size of the planet from the star. Inside the angle $2\alpha$ the moon is eclipsed by the planet. The eclipsing fraction is thus defined as fraction of the orbit which is in shadow, $\epsilon = 2\alpha/2\pi$.

a minimum ocean fraction of $f_{\text{ocean, min}} = 36\%$. Similar to the eccentricity case, high obliquities can partially recover from the snowball. In this case it is due to the pole facing the Sun melting for half a year due to constant insolation before refreezing when facing away from the Sun. There are nearly no variations due to changing ocean fraction above $f_{\text{ocean}} = 20\%$ in the eccentricity case, and few variations above $f_{\text{ocean}} = 40\%$ for the obliquity case.

## 4. EARTH-LIKE EXOMOON MODIFICATIONS AND INVESTIGATIONS

### A. Eclipsing

In order to add eclipsing to the model it must be known when the moon is behind the gas giant such that the sun is blocked. When modelling eclipsing, the gas giant and moon are assumed to have co-planar orbits such that the full radius of the gas giant is used. It is also assumed that in the umbra the moon is fully eclipsed, and in the penumbra the moon is half eclipsed. In reality the penumbra varies between 0% eclipsed at the outer edge to 100% eclipsed at the edge to the umbra.

Initially, the eclipsing was quantified by solving for the distances and angles of the gas giant and moon using eqns. (24) and (25). The eccentric anomaly, $E$, is related to the true anomaly, $\nu$, by,

$$\cos\nu = \frac{\cos E - e}{1 - e\cos E}, \tag{38}$$

where $e$ is the eccentricity of the orbit. By finding the x-y coordinates of the gas giant and moon, when the moon is eclipsed can be found. Due to the length of the eclipses a time step of an hour must be used to evolve this eclipsing model. This would be impractical to run alongside the 1-day time step of the EBCM especially as the iteration process for finding the eccentric anomaly is time-consuming. Varying the 4 orbital parameters in the eclipsing model gives insight into the variables affecting the eclipsing. Varying the eccentricity of the gas giant between $0$ and $0.9$ has a random effect on the eclipsing between the values $5\%$ and $5.2\%$, and increasing eccentricity

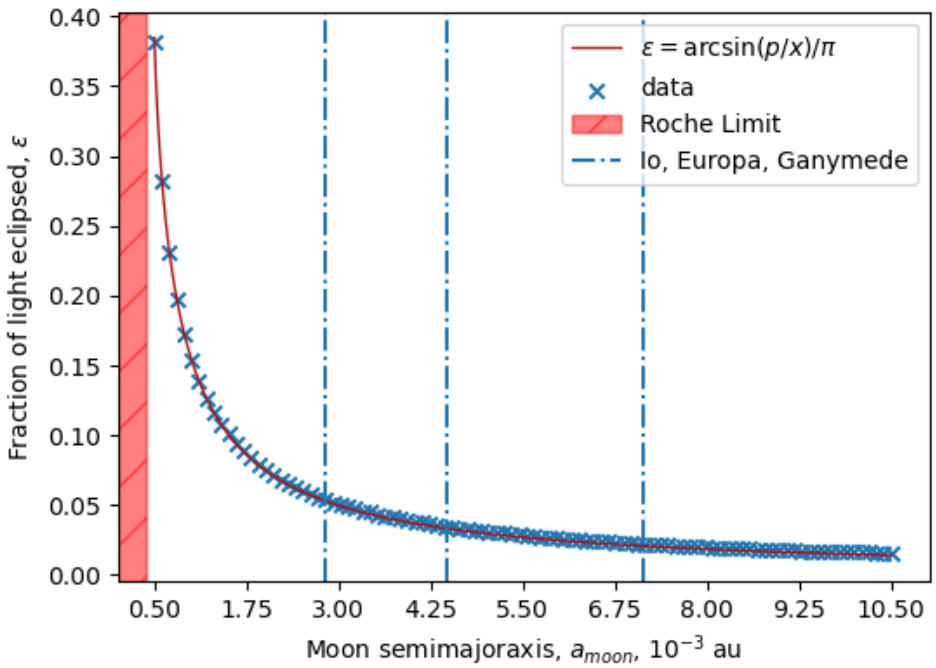


**FIG. 12:** Fraction of light eclipsed by a Jupiter sized gas giant when varying a moon's semi-major axis. Shown is the Roche limit for Jupiter, as well as the orbital distances of Jupiter's three innermost moons. Overlaid on the data is a fit of $\epsilon = \arcsin(p/x)/\pi$ with parameter $p = (4.675 \pm 0.005) \times 10^{-4}$ au.

of the moon from $e = 0$ to $0.1$ decreases the eclipsing from $5.07\%$ to $5.02\%$. Likewise, varying the gas giant semi-major axis between $0.5$ au and $10$ au caused variation in the eclipsing fraction between $5\%$ and $6\%$. The most important influence to the eclipsing was moon semi-major axis. Varying between $0.5$ mau and $10.5$ mau caused a decrease in eclipsing from $40\%$ to $2\%$ as seen in Fig. 12.

Knowing that the eccentricity of the orbits makes a negligible contribution to the motivates an analytical model with circular orbits. Using the assumption that the sun is a point source (valid if $a_{\text{gas}} \gg 10a_{\text{moon}}$, which is true in the cases considered in this paper) the diagram shown in Fig. 11 is drawn and used to quantify the eclipsing fraction as follows.

In order to find the eclipsing angle, $\alpha$, the distances $x$ and $y$ need to be found. The $x$ distance relates the angular size of the gas giant from the sun, $\theta$, to the eclipsing angle as

$$x = a_{\text{moon}} \sin\alpha = (a_{\text{gas}} + y) \tan\theta, \tag{39}$$

where the distance $y = a_{\text{moon}} \cos\alpha$ using the smaller triangle. Using the larger triangle, the angular size of the gas giant can also be found to be

$$\sin\theta = \frac{R_{\text{gas}}}{a_{\text{gas}}}, \tag{40}$$

which can then, in the small angle approximation that $\sin\theta = \tan\theta$, be related to the $\tan\theta$ term in eqn. (39). This leads to the relation of eclipsing angle to the radius of gas giant, and semimajor axes of the moon and gas giant as follows,

$$\frac{R_{\text{gas}}}{a_{\text{moon}}} + \frac{R_{\text{gas}}}{a_{\text{gas}}} \cos\alpha = \sin\alpha. \tag{41}$$

This equation can be solved for the eclipsing angle in the sine term by using that $R_{\text{gas}} \ll a_{\text{gas}}$ so ignoring the cosine term. The eclipsing fraction, $\epsilon$, can then be found by dividing 2 times the eclipsing angle by the full orbital angle $2\pi$

$$\epsilon = \frac{2\alpha}{2\pi} = \frac{1}{\pi} \arcsin \frac{R_{\text{gas}}}{a_{\text{moon}}}. \tag{42}$$

This relation is investigated in Fig. 12 with a free parameter in place of $R_{\text{gas}}$. The value of the free parameter is $(7.013 \pm 0.008) \times 10^7$m which is extremely close to the radius of Jupiter, as to be expected.

### B. Reflectance and Emission from the Gas Giant

Two sources of heat are indirectly from the star via the gas giant. First, light from the star can be reflected by the gas giant. The light absorbed by the gas giant is given by $S(1 - A_{\text{gas}})$, thus light reflected is given by $SA_{\text{gas}}$. This must be reduced by the distance, $a_{\text{moon}}$, and the eccentricity, $e_{\text{moon}}$, of the moon's orbit,

$$F_{\text{ref}} = \frac{SA_{\text{gas}}}{4\pi a_{\text{moon}}^2 \sqrt{1 - e_{\text{moon}}^2}}, \tag{43}$$

where $S = 1360$ Wm$^{-2}$ is the same insolation as for the moon. The $4\pi a^2\sqrt{1-e^2}$ term in the denominator comes from eqn. (36) for average flux from a body. Second, IR emission from the gas giant can heat up the moon. This IR emission can have two sources, the first and most obvious is the gas giant being heated by the star and then reradiating that heat in equilibrium. This can be described using the 0DEBM (eqn. (1)) as

$$F_{\text{emit}} = \frac{4\pi R_{\text{gas}}^2 \sigma T_{\text{gas}}^4}{4\pi a_{\text{moon}}^2 \sqrt{1 - e_{\text{moon}}^2}} = \frac{R_{\text{gas}}^2 S(1 - A_{\text{gas}})}{4a_{\text{moon}}^2 \sqrt{1 - e_{\text{moon}}^2}}, \tag{44}$$

where this flux assumes that the gas giant is in equilibrium as expected by the 0DEBM with the variables given in Table. II. An alternative source is residual heat of formation. For example, Jupiter is still slightly warmer than expected from equilibrium [21]. This is not accounted for in this model, but could be added by setting the temperature directly instead of using the 0DEBM.

### C. Tidal Heating

In the fixed-Q model, $-\text{Im}(k_2) = k_2/Q$, where $k_2$ is the second Love number for the moon and $Q$ is the total dissipation factor due to friction, with both numbers constant. This model has some failings. The second Love number depends on material properties of the moon so will be directly influenced by the temperature of the mantle and core. These temperatures are also directly influenced by the amount of flux the moon receives due to tidal and radiogenic heating. This model is not responsive to this dynamic temperature dependence and requires a single temperature of the core to be picked.

Alternatively, viscoelastic models allow for the core temperature to vary with respect to the amount of flux from tidal heating. To do this the stable point where tidal flux is equal to convective cooling for the core is found. Both the tidal heat and convective cooling are dependent

| Moon | | | | Gas Giant | | |
|---|---|---|---|---|---|---|
| Semi-major axis | Eccentricity | Radius | Density | Mass | Radius | Albedo |
| 0.03 au | 0.006 | $6.4 \times 10^6$ m | 5500 kg m$^{-3}$ | $1.9 \times 10^{27}$ kg | $7.0 \times 10^7$ m | 0.3 |

**TABLE II:** A summary of the default parameters for the Earth-like exomoon model. The moon orbital parameters are ones which generate a good level of tidal heating, and the radius and density are similar to the radius and density of the Earth. The gas giant parameters are the same as Jupiter's [30], where the volumetric mean radius, and bond albedo have been used. Other model parameters are the same as the planetary model (Tab. I).

on temperature of the core, thus this method finds temperature of the core at equilibrium. The implicit assumption here is that the moon has been in orbit long enough to have reached equilibrium between the tidal heating and convective cooling. This paper uses the Maxwell model from Henning et al [26], given by

$$-\text{Im}(k_2) = \frac{57\eta\omega}{4\beta\left[1 + \left(1 + \frac{19\mu}{2\beta}\right)^2 \left(\frac{\eta\omega}{\mu}\right)^2\right]} \tag{45}$$

where $\beta = \rho g R_{\text{moon}}$ has been described as gravitational stiffness term with $\rho$ being the density of material in the moon, $g$ being the moon's surface gravity, and $R$ being the radius of the moon. The temperature dependent forms of the viscosity, $\eta$, and shear modulus, $\mu$, are given in Henning et al [26] and in appx. B. The orbital frequency, $\omega$, and other parameters take (or can be derived from) the default values in Tab. II.

The tidal heating can sharply cut off for certain orbital parameters when the tidal heating is less than convective cooling at all mantle temperatures, so the core temperature at equilibrium is too low to heat the surface of the planet effectively.

### D. Impact on Previous Investigations

With the model appropriately updated, temperature profiles and habitabilities seen previously can be investigated for this moon model. Shown in Fig. 13 is how the time-averaged (HC) habitability for variable semi-major axis changes between the planetary model and moon model (left) and how the equilibrium temperature changes with semi-major axis (right). The plot on the left shows how the latitude habitable zone changes between a planetary model and a moon model with the default parameters in Tab. II. And the plot on the right shows how the equilibrium temperature of the planet between the planetary model and two moon models, one with default parameters and one with higher lunar eccentricity.

In the latitude plot the habitable zone becomes wider at all latitudes and moves outwards towards Mars' orbit. The reason for both these effects is the additional energy flux from tidal heating. The habitable zone becomes wider as the moon is less reliant on a specific distance from the Sun to generate habitable temperatures, and the habitable zone moves further out as the additional energy flux generally raises the temperature of the planet, meaning it is too hot for life at the closer distances. This means that exomoons which are found at distances further from their host stars than are habitable for planets may still be habitable due to tidal heating.

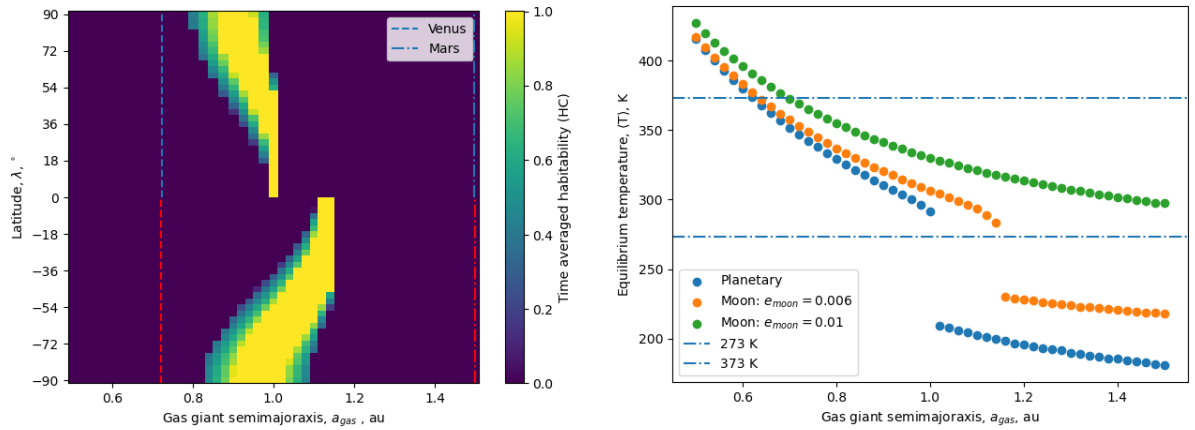


**FIG. 13:** Left: Comparison of the time-averaged (HC) habitability for variable semi-major axis for the planetary model (top) and moon model (bottom). The moon model has the default parameters in Tab. II. Right: Comparison of the equilibrium temperatures when varying gas giant semi-major axis for the planetary model (blue), and two moon models with different eccentricity (orange and green). Also shown are horizontal lines for the freezing and melting points of water.

This is also seen in the equilibrium temperatures, where a wider range of values are within the range for liquid water. Seen in the orange set of data is a more exaggerated curve when falling to the snowball state than for the planetary model in blue. This is due to IAF playing less of a role in determining the climate of the planet as the tidal heating is independent of albedo. The tidal heating also helps to prevent the planet's temperature from decreasing to the point where IAF can dominate by providing a constant heat source when further from the star. At higher lunar eccentricities it is possible for the moon to have completely habitable temperatures without the need for a star, which means that exomoons orbiting a rogue gas giant without a star may have a chance to harbour life.

Similarly, in Fig. 14 the equilibrium temperatures when varying gas giant eccentricity (left) and planetary obliquity (right) with different moon eccentricities are shown. The dip in temperature at low eccentricity due to IAF is missing from the moon models. This is because temperatures are generally higher so the IAF cannot start. In the obliquity case the characteristic 'S' shape of the temperature with increasing obliquity is reduced in two ways. First is that the inflection point of the curve moves to higher obliquities, and second that the range in temperature decreases from the planetary model to the moon models. Both these changes indicate that the moon model depends less on the obliquity of the planet to inform its climate, mostly due to the tidal heating meaning that the poles are melted much more easily and have trouble forming without the help of IAF.

### E. Exomoon Semi-major Axis and Eccentricity Investigations

In Fig. 15 the HC time-averaged habitability for each latitude band is shown when varying the moon's semi-major axis (left) and eccentricity (right).

Variable moon semi-major axis has a similar shape to the variable gas semi-major axis, though the scaling is much sharper due to the insolation scaling as $a_{\rm gas}^{-2}$ and the tidal heating

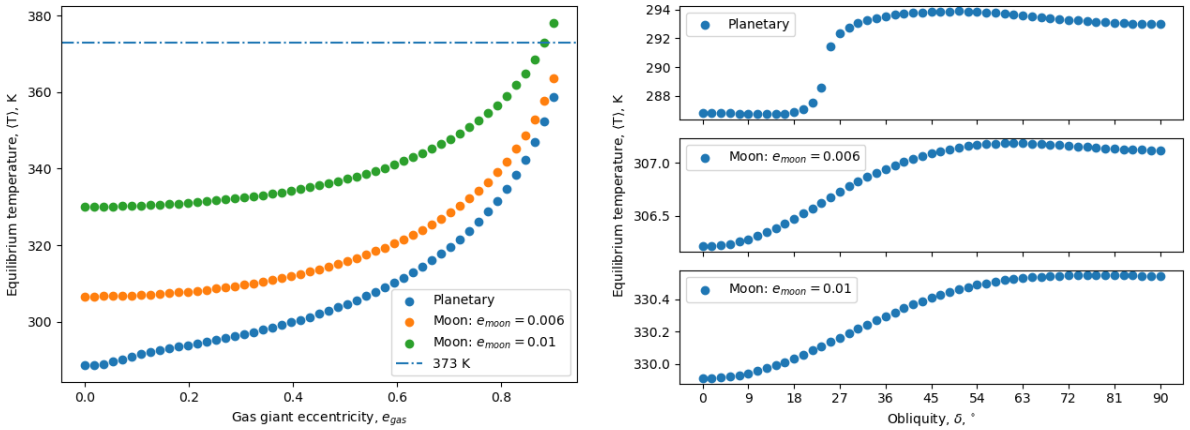


**FIG. 14:** Left: Comparison of the equilibrium temperatures when varying eccentricity for the planetary model (blue), and when varying gas giant eccentricity two moon models with different moon eccentricities (orange and green). Right: Comparison of the equilibrium temperatures when varying obliquity for the planetary model (top) and two moon models with different eccentricity (middle and bottom). The y-axes are very different, as each has progressively smaller range in values.

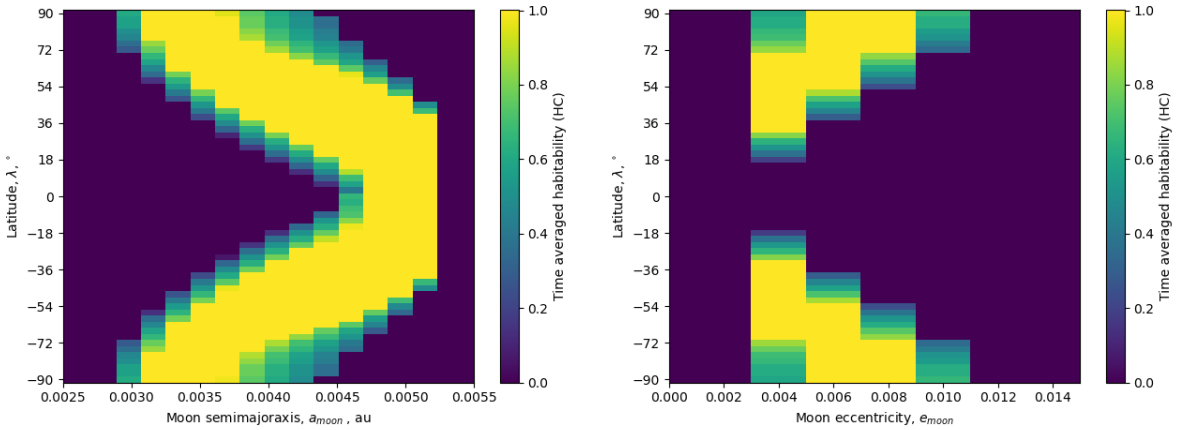


**FIG. 15:** Left: Time-averaged temperature heat map for each latitude band when varying moon semi-major axis. Right: Time-averaged temperature heat map for each latitude band when varying moon eccentricity.

scaling as $a_{\text{moon}}^{-15/2}$. At high semi-major axis the tidal heating is less than the convective cooling, so 'turns off'. It might be expected that a moon in orbit around a gas giant at the same distance as the Earth from the Sun would still be warm enough to be habitable. However, these graphs show how when the tidal heating switches off the moon does not receive enough insolation so falls into a snowball state. This is because to the reduction of insolation due to eclipsing is larger than the additional light reflected and emitted from the gas giant. As shown in Fig. 4 even a small decrease in insolation, such as the decrease due to eclipsing, can lead to a snowball state.

Variable moon eccentricity is quite different to the gas giant eccentricity. At very low eccentricity the tidal heating turns off, so the moon falls into a snowball as already described. At high eccentricity the tidal heating is strong enough to raise the temperature of the moon by a large

amount. The key difference is that the gas giant eccentricity must reach $0.8$ before rendering the planet completely uninhabitable, whereas the moon eccentricity can raise temperature to uninhabitable levels at only $e_{\text{moon}} = 0.01$.

## 5. DISCUSSION

In modelling the habitability of these exoplanets and exomoons a number of assumptions were made.

This model assumes that there is a thick atmosphere capable of transporting heat across the surface of the planet (i.e. between and within latitude bands). This may not be true for all exoplanets, but a reasonable expectation of a habitable exoplanet would be a breathable atmosphere, so this assumption is most likely valid. However, something not considered with the atmospheric dynamics is the effect of high temperature on rate of atmosphere loss and water loss. When looking at the extreme temperature variations caused by a highly eccentric orbit the planet may reach temperatures in excess of $200°$C when close to the star and cool to temperatures of $30°$C when far from the star. It would be expected that the high temperature would boil away much of the atmosphere and oceans, however this model does not take this into consideration. This is somewhat handled by the HC habitability function not allowing for extreme temperatures, but can lead to misleading average temperatures where the planet looks to be within a habitable temperature when the variation in temperature is very large. Future work on the model could include additional climate modelling beyond just temperature, such as adding a hydrological cycle and carbon-silicate cycle as well as atmospheric loss due to temperature. These would investigate more closely the evolution of the atmosphere and how that impact the habitability of the model.

The approximation of a uniform planet could also be probed further. Exoplanets may have land-ocean distributions similar to Earth where the Northern Hemisphere has more land than the Southern Hemisphere. The planet could be probed with different fractions of land and ocean. For example: an ocean centred on one of the poles of the planet and increasing in size from a desert world with small a polar ocean to ocean world with a small polar continent. Further, the ocean for the planet is assumed to have the same mixing depth at all points, and the planet is assumed to have uniform altitude across its entire surface. These assumptions do not impact the model too much when considering an exoplanet whose surface features are not known, however in the future (or when modelling the Earth for example) these values must be examined for carefully.

Research motivated by climate change suggests that ice melting can release $CO_2$ which is not accounted for in this model. This would introduce an ice-temperature feedback where melting ice releases $CO_2$, increasing greenhouse gas effects and feeding back until the temperature is very high. This would reduce the habitability at higher temperatures particularly where the icecaps melt due to a higher $CO_2$ fraction in the atmosphere, thus larger greenhouse effect. However, this effect is very particular for the Earth due to its $CO_2$ rich past. It would not be correct to assume that all exoplanets have a $CO_2$ rich past but could be considered in further research.

In order to relax the assumption of a diurnally averaged insolation the longitude dimension

must be added to the model. This would allow for a closer examination of heat flow across the planet, as well as potentially allow for analysis of tidally locked planets or planets with very slow rotation. Analysis of tidally locked planets would be of particular relevance due to many exoplanets detected around cooler red stars being tidally locked. Also, the insolation in the model is dependent only on semi-major axis, obliquity, and eccentricity. Further work could include varying the insolation to follow the Sun's sunspot cycle to investigate how this could affect the climate. For example, a solar minimum may be enough in some cases to cause the planet to fall into a snowball state which is not reflected in the current model.

The tidal heating for the moon model varies slightly with surface temperature but is roughly constant in time. This assumption is valid for low eccentricities due to the time taken for heat to travel from core to surface. At much higher lunar eccentricities ($e_{\text{moon}} > 0.1$) the time for heat to be injected to the core (and amount that is injected) means that this assumption no longer holds. Modelling this time dependent tidal heating may allow for more in-depth modelling of exomoon systems. A counter to this is that high eccentricity moons very quickly circularise their orbits due to orbital energy being transferred to the planet interior via tidal heating. This means that the only exomoons with stable eccentric orbits which allow for tidal heating are those which have low eccentricities and have orbital resonances to maintain that eccentricity Thus, the powerful tidal heating at high eccentricity is important for early formation but not for later evolution.

Eclipsing in the model is independent of eccentricity of the orbit of the gas giant and moon. Further work with this model could include eccentricity, either through an analytical approach or by improving the speed and accuracy of the orbit simulation code. Another assumption made when modelling the eclipsing was that the star was point-like. In most regimes this is an effective assumption but could also be relaxed to further enhance the model.

All the exomoons considered in this paper have eccentric orbits at small semi-major axes. These values were chosen to highlight the effect that tidal heating had on the moon and its habitability. Further work could focus on exomoons which are not tidally heated as this would allow for the effects of the light from the gas giant and the eclipsing to be more apparent. If the orbital code were improved then the time dependent nature of the eclipsing could be investigated to determine any time dependent effects on the habitability of the moon.

Alternatively, the tidal heating of the moon could be focused on more. A 'depth model' could be devised from the heat equation by allowing radius to vary with the angles constant. This would allow for a more rigorous investigation of how the tidal heat flows outwards from the core. An application of this depth model would be for a moon like Io or Titan which has a frozen outer shell with potential for a liquid water ocean under which could be melted and maintained by tidal heat. The investigation would then follow a similar one to this paper where the potential for habitable temperatures could be investigated by varying the parameters of the model.

## 6. CONCLUSION

The habitability of a latitude band model of Earth-like exoplanets and exomoons has been investigated when varying orbital and planetary parameters.

A relationship derived from average insolation to a planet was found to describe the scaling of average temperature with semi-major axis and eccentricity which can be used to estimate habitability. However, it was also shown that eccentricity means the variation in temperature can be too large to sustain life. Further, it was investigated how these relationships are influenced when switching to a moon model with tidal heating, eclipsing, and light from the parent body.

The susceptibility of the model to runaway ice-albedo-feedback was also investigated and found to occur for reduced insolation due to sightly larger semi-major axis, as well as variable insolation due to eccentricity and obliquity when at low ocean fraction. Obliquity was found to require a higher minimum ocean fraction than eccentricity (40% to 20%) to prevent runaway ice-albedo-feedback, indicating that obliquity has the larger role in determining if a planet is in a 'snowball state'. It was found that Earth's current orbital and planetary parameters mean the planet experiences some ice-albedo-feedback which seen primarily in the frozen poles but also in Earth's history of ice ages.

## REFERENCES


[1] ESA. A brief introduction to exoplanets. https://sci.esa.int/web/exoplanets/-/60654-a-brief-introduction-to-exoplanets. Accessed: 2024/03/05, Last updated 2019/09/01.

[2] D. Nesvorný, D. Kipping, D. Terrell, et al. The Astrophysical Journal, 777(1), 2013. doi: 10.1088/0004-637X/777/1/3.

[3] K. M. Lewis, P. D. Sackett, and R. A. Mardling. The Astrophysical Journal, 685(2), 2008. doi: 10.1086/592743.

[4] D. M. Kipping, S. J. Fossey, and G. Campanella. Monthly Notices of the Royal Astronomical Society, 400(1), 2009. doi:10.1111/j.1365-2966.2009.15472.x.

[5] M. A. Limbach and E. L. Turner. The Astrophysical Journal, 769(2), 2013. doi:10.1088/0004-637X/769/2/98.

[6] M. A. Limbach, J. M. Vos, J. N. Winn, et al. The Astrophysical Journal Letters, 918(2), 2021. doi:10.3847/2041-8213/ac1e2d.

[7] Exoplanet Team. https://exoplanet.eu. Accessed: 2024/03/05, Last update: 2024/03/04.

[8] NASA. Artemis plan. https://www.nasa.gov/specials/artemis/. Accessed: 2024/03/06.

[9] CNSA. Construction of the international lunar research station. https://www.cnsa.gov.cn/english/n6465652/n6465653/c6811380/content.html. Accessed: 2024/03/06.

[10] M. Gillon, A. Triaud, B.-O. Demory, et al. Nature, 542(7642), 2017. doi:10.1038/nature21360.

[11] O. Cohen, A. Glocer, C. Garraffo, et al. The Astrophysical Journal, 962(2), 2024. doi: 10.3847/1538-4357/ad206a.

[12] G. Van Looveren, M. Güdel, S. Boro Saikia, et al. Astronomy & Astrophysics, 683, 2024. doi: 10.1051/0004-6361/202348079.

[13] G. R. North and J. A. Coakley. Journal of Atmospheric Sciences, 36(7), 1979. doi:10.1175/1520-0469(1979)036¡1189:DBSAMA¿2.0.CO;2.

[14] D. M. Williams and J. F. Kasting. Icarus, 129(1), 1997. doi:10.1006/icar.1997.5759.

[15] D. S. Spiegel, K. Menou, and C. A. Scharf. The Astrophysical Journal, 681(2), 2008. doi: 10.1086/588089.

[16] D. S. Spiegel, K. Menou, and C. A. Scharf. The Astrophysical Journal, 691(1), 2009. doi: 10.1088/0004-637X/691/1/596.

[17] C. D. Dressing, D. S. Spiegel, C. A. Scharf, et al. The Astrophysical Journal, 721(2), 2010. doi: 10.1088/0004-637X/721/2/1295.

[18] Y.-C. Lu and D. M. Romps. Environmental Research Letters, 18(9), 2023. doi:10.1088/1748-9326/ace83c.

[19] D. M. Williams, J. F. Kasting, and R. A. Wade. Nature, 385, 1997.

[20] D. M. Williams. Astrobiology, 13 4, 2013.

[21] L. Li, X. Jiang, R. A. West, et al. Nature Communications, 9, 2018.

[22] C. F. Yoder and S. J. Peale. Icarus, 47(1), 1981. doi:10.1016/0019-1035(81)90088-9.

[23] M. Segatz, T. Spohn, M. Ross, et al. Icarus, 75(2), 1988. doi:10.1016/0019-1035(88)90001-2.

[24] V. Dobos and E. L. Turner. The Astrophysical Journal, 804(1), 2015. doi:10.1088/0004-637X/804/1/41.

[25] V. Dobos, R. Heller, and E. L. Turner. The American Astronomical Society, 601, 2017. doi: 10.1051/0004-6361/201730541.

[26] W. G. Henning, R. J. O'Connell, and D. D. Sasselov. The Astrophysical Journal, 707(2):1000, 2009. doi:10.1088/0004-637X/707/2/1000.

[27] J. Laskar, A. Fienga, M. Gastineau, et al. Astronomy & Astrophysics, 532, 2011. doi: 10.1051/0004-6361/201116836.

[28] A. Méndez and E. G. Rivera-Valentín. The Astrophysical Journal Letters, 837(1), 2017. doi: 10.3847/2041-8213/aa5f13.

[29] C. Emiliani. Earth and Planetary Science Letters, 37(3), 1978. doi:10.1016/0012-821X(78)90050-X.

[30] NASA. Jupiter fact sheet. `https://nssdc.gsfc.nasa.gov/planetary/factsheet/jupiterfact.html`. Accessed: 2024/03/01.

[31] V. Hansteen. Numerical modelling in a nutshell. `https://www.uio.no/studier/emner/matnat/astro/AST5110/h11/undervisningsmateriale/numerics_intro.pdf`. Accessed: 2023/11/06.

## Appendix A: Numerical Stability of the 1DEBCM

The general stability of the model can be understood by following the recipe provided in "Numerical Modelling in a nutshell" [31]. The model is however quite complex and does not easily yield to the methods provided, so approximations such as requiring an equilibrium state must be used which mean we achieve lower bounds for the instability.

Assume the PDE can be solved with a plane wave solution of the form

$$T_n^m = \xi^n \exp ikm\Delta\lambda \tag{A1}$$

where $\xi$ is a (complex) scaling factor which determines the growth characteristics of the plane wave, $n$ and $m$ are the time and space indices respectively, and $k$ is the spatial frequency of the plane wave.

Taking this plane wave solution and substituting it into (2) after being discretised, dividing by the plane wave and using the definition of $\sin(x)$ in terms of exponentials we arrive at,

$$\xi(k) = 1 + \Delta t \left\{ \frac{f_n^m}{t_n^m} + i g_n^m \tan\lambda_m \frac{\sin(k\Delta\lambda)}{\Delta\lambda} - g_n^m \frac{\sin^2(k\Delta\lambda)}{(\Delta\lambda)^2} \right\} \tag{A2}$$

where $f_n^m = (S(1-A) - I)/C$ and $g_n^m = D/C$.

In an equilibrium system the $f_n^m$ term equals $0$ as the input energy and output energy of the system are equal. Of course an equilibrium state will not be reached if the integration is unstable, so this analysis will give a lower bound to where the instabilities of the model should occur.

Instability occurs when the scaling factor has magnitude greater than 1, $|\xi|^2 > 1$, leading to an instability criterion of

$$g\Delta t \left( \tan^2(\lambda_m) + \frac{\sin^2(k\Delta\lambda)}{(\Delta\lambda)^2} \right) > 2, \tag{A3}$$

suggesting that heat capacity, diffusivity, time step, spatial step, and position on the PDE all contribute to instability.

Considering the equator of the model at $\lambda_m = 0$. The $\tan\lambda_m$ term equals $0$, so the instability simplifies to

$$g\Delta t \frac{\sin^2(k\Delta\lambda)}{\Delta\lambda} > 2, \tag{A4}$$

it is known that $\sin^2(x) \in [0,1]$ so if $g\Delta t/(\Delta\lambda)^2 < 2$ then the model will be stable at the equator for all frequencies.

Solving for $\Delta\lambda$ in this case:

$$\Delta\lambda > \sqrt{\frac{\Delta t g}{2}} \tag{A5}$$

We may then use this equation to find the lower bound for the system will be unstable. We can set the time step to $\Delta t = 1$ day and $g = D/C$ with $D = 0.56$ Jm$^{-2}$ s$^{-1}$ K$^{-1}$. The heat capacity $C$ will however be variable, depending on land-ocean fraction and ocean-ice fraction.

For the land-only system the heat capacity is at it's lowest at $C = 5.25 \times 10^6$J m$^{-2}$K$^{-1}$. This gives a value for $g$ of $1.07 \times 10^{-7}$s$^{-1}$, thus

$$\Delta\lambda \geq \sqrt{\frac{24 \times 60 \times 60 \times 1.07 \times 10^{-7}}{2}} = 0.068^{\text{rad}} = 3.9^\circ$$

is always stable. The opposite end of the spectrum is the ocean-only system with no ice, where the heat capacity has value $C = 40C_{\text{land}}$, reducing the tolerance to $\Delta\lambda \geq 0.6°$. The value for the $f_{\text{ocean}} = 0.7$ ocean to land model is roughly $4 \times 0.3 + 0.6 \times 0.7 = 1.62°$. The instability in the actual model can be found by varying the spatial dimension (thus $\Delta\lambda$), as seen in Figure 16. The instability occurs around $\Delta\lambda \approx 1.23°$ which is reasonably close to the calculated value.

**FIG. 16:** The convergence of a series of Earth-like models with varying spatial dimension (x-axis). Top: The time in years for the system to converge to a steady temperature, Bottom: the temperature converged to. The values of time and temperature of $-1$ and $0$ respectively are when the model breaks and diverges to infinity. The model breaks around $1.23°$ separation (146 spatial nodes) in rough agreement with the calculated value of $1.62°$.

The discretisation of the model at the poles is slightly different (see eqns. (30) and (31)). Looking only at the South Pole (though the North Pole is much the same) and plugging in (A1) into (30),

$$\frac{\xi^{n+1} - \xi^n}{\Delta t} = g\frac{\xi^n \exp(ik\Delta\lambda) - \xi^n}{(\Delta\lambda)^2} \tag{A6}$$

Dividing by (A1) and solving for $\xi$ we find,

$$\xi = 1 + \frac{g\Delta t}{(\Delta\lambda)^2}\left(\exp(ik\Delta\lambda) - 1\right) \tag{A7}$$

Leading to an absolute square magnitude given by

$$|\xi|^2 = 1 + 2(1 - \cos(k\Delta\lambda))\frac{g\Delta t}{\Delta\lambda^2}\left(\frac{g\Delta t}{\Delta\lambda^2} - 1\right) \tag{A8}$$

Which means the poles of the model are stable when $|\xi|^2 \leq 1$:

$$\begin{aligned} 0 &\geq 2(1 - \cos(k\Delta\lambda))\frac{g\Delta t}{\Delta\lambda^2}\left(\frac{g\Delta t}{\Delta\lambda^2} - 1\right) \\ 0 &\geq \frac{g\Delta t}{\Delta\lambda^2} - 1 \\ 1 &\geq \frac{g\Delta t}{\Delta\lambda^2} \\ \Delta\lambda &\geq \sqrt{g\Delta t} \end{aligned}$$

using at first that $\cos(x) \in [-1, 1]$ and that $g\Delta t/\Delta\lambda^2 > 0$. This is a stricter stability criteria than for the equator by a factor of $\sqrt{2}$, which is why the poles are usually the issue causing the model to diverge to infinity when the equator is fine. It is also true that if $\cos(k\Delta\lambda) = 1$ then the model is always stable at the poles. However, this corresponds to a trivial constant state $k = 0$ or a non-computational separation of $0$ so is not of interest.

**Appendix B: Tidal Heating Equations and Method**

$$\eta = \begin{cases} \eta_0 \exp\left(E_a/RT\right) & T < T_s \\ \eta_0 \exp\left(E_a/RT\right) \exp\left(-B\phi\right) & T_s < T < T_b \\ 10^{-7} \exp\left(40000\text{K}/T\right)(1.35\phi - 0.35)^{-5/2} & T_b < T < T_l \\ 10^{-7} \exp\left(40000\text{K}/T\right) & T_l < T \end{cases} \tag{B1}$$

$\eta_0 = 1.6 \times 10^5$ Pa s $T_s = 1600$ K $T_l = 2000$ K $T_b = T_s + f(T_l - T_s) = 1800$ K for $f = 0.5$ $E_a = 3 \times 10^5$ J.mol$^{-1}$

$$\mu = \begin{cases} 5 \times 10^{10} & T < T_s \\ 10^{\frac{8.2 \times 10^4 \text{K}}{T} - 40.6} & T_s < T < T_b \\ 10^{-7} & T_b < T \end{cases} \tag{B2}$$

## SCIENTIFIC SUMMARY FOR A GENERAL AUDIENCE

Many interesting solar systems have been reported in the news, such as the Trappist-1 system which is filled with Earth-like planets. Simulations and models such as those in this paper are used to determine if a planet could be habitable. A habitable zone can be made by varying the parameters of the model to see where the model is habitable, partially habitable, or uninhabitable.

The main model in this paper takes a planet and divides it into a number of latitude bands which can have energy flow between them. Certain parameters, such as how the planet orbits around its star and the angle the planet is tilted at, are varied to build this habitable zone. A result of this paper is if the Earth orbited slightly further away from the Sun then it is likely that it would fall into an ice age similar to what the Earth has experienced in the past. Another result found is that the tilt of the planet can affect how hot or cold it is, and indicates that the current tilt of the Earth gives a cold planet.

Another aspect of this paper's exoplanet research is exomoons orbiting a gas giant such as Jupiter. In certain configurations an exomoon can be heated not only from the host star, but also due to a process called tidal heating. Tidal heating is similar to stretching an elastic band. Stretching and relaxing an elastic band many times can cause the band to warm up. The moon of a gas planet is stretched slightly by unequal forces of gravity as one part of the moon is further away than the other. If the moon's orbit is not circular then the moon is stretched and relaxed, thus heats up in a similar way to the elastic band. Adding tidal heating to the model allows for investigations into how tidal heating can move, or change the shape of, the habitable zone.